

# Current Biology

## A Retino-retinal Projection Guided by Unc5c Emerged in Species with Retinal Waves

### Highlights

- A subset of retinal ganglion cells project to the contralateral retina
- Unc5c mediates the formation of the retina-retina projection
- Unc5c retinal expression correlates with extent of refinement in visual targets
- Congruency of visual maps in species with retinal waves may rely on R-R axons

### Authors

Verónica Murcia-Belmonte,  
Yaiza Coca, Celia Vegar, ...,  
Luis M. Martinez, Lynda Erskine,  
Eloísa Herrera

### Correspondence

e.herrera@umh.es

### In Brief

Murcia-Belmonte et al. demonstrate the existence of an Unc5c-dependent transient projection that connects both retinas in several vertebrate species. Computational modeling suggests this retina-retina projection may be critical for the congruency of visual maps in species that undergo retinal wave-dependent axon refinement during development.



# A Retino-retinal Projection Guided by Unc5c Emerged in Species with Retinal Waves

Verónica Murcia-Belmonte,<sup>1</sup> Yaiza Coca,<sup>1</sup> Celia Vegar,<sup>1</sup> Santiago Negueruela,<sup>1</sup> Camino de Juan Romero,<sup>1</sup> Arturo José Valiño,<sup>1</sup> Salvador Sala,<sup>1</sup> Ronan DaSilva,<sup>2</sup> Artur Kania,<sup>2,3</sup> Víctor Borrell,<sup>1</sup> Luis M. Martínez,<sup>1</sup> Lynda Erskine,<sup>4</sup> and Eloísa Herrera<sup>1,5,\*</sup>

<sup>1</sup>Instituto de Neurociencias, Consejo Superior de Investigaciones Científicas-Universidad Miguel Hernández, CSIC-UMH, Av. Santiago Ramón y Cajal s/n, Sant Joan d'Alacant 03550, Alicante, Spain

<sup>2</sup>Institut de Recherches Cliniques de Montréal (IRCM), 110, ave. des Pins Ouest, Montréal, QC H2W 1R7, Canada

<sup>3</sup>Division of Experimental Medicine, Department of Anatomy and Cell Biology, McGill University, Montréal, QC H3A 2B2, Canada

<sup>4</sup>School of Medicine, Medical Sciences and Nutrition, Institute of Medical Sciences, University of Aberdeen, Aberdeen AB25 2ZD, Scotland, UK

<sup>5</sup>Lead Contact

\*Correspondence: [e.herrera@umh.es](mailto:e.herrera@umh.es)

<https://doi.org/10.1016/j.cub.2019.02.052>

## SUMMARY

The existence of axons extending from one retina to the other has been reported during perinatal development in different vertebrates. However, it has been thought that these axons are either a labeling artifact or misprojections. Here, we show unequivocally that a small subset of retinal ganglion cells (RGCs) project to the opposite retina and that the guidance receptor *Unc5c*, expressed in the retinal region where the retinal-retinal (R-R) RGCs are located, is necessary and sufficient to guide axons to the opposite retina. In addition, *Netrin1*, an *Unc5c* ligand, is expressed in the ventral diencephalon in a pattern that is consistent with impeding the growth of *Unc5c*-positive retinal axons into the brain. We also have generated a mathematical model to explore the formation of retinotopic maps in the presence and absence of a functional connection between both eyes. This model predicts that an R-R connection is required for the bilateral coordination of axonal refinement in species where refinement depends upon spontaneous retinal waves. Consistent with this idea, the retinal expression of *Unc5c* correlates with the existence and size of an R-R projection in different species and with the extent of axonal refinement in visual targets. These findings demonstrate that active guidance drives the formation of the R-R projection and suggest an important role for these projections in visual mapping to ensure congruent bilateral refinement.

## INTRODUCTION

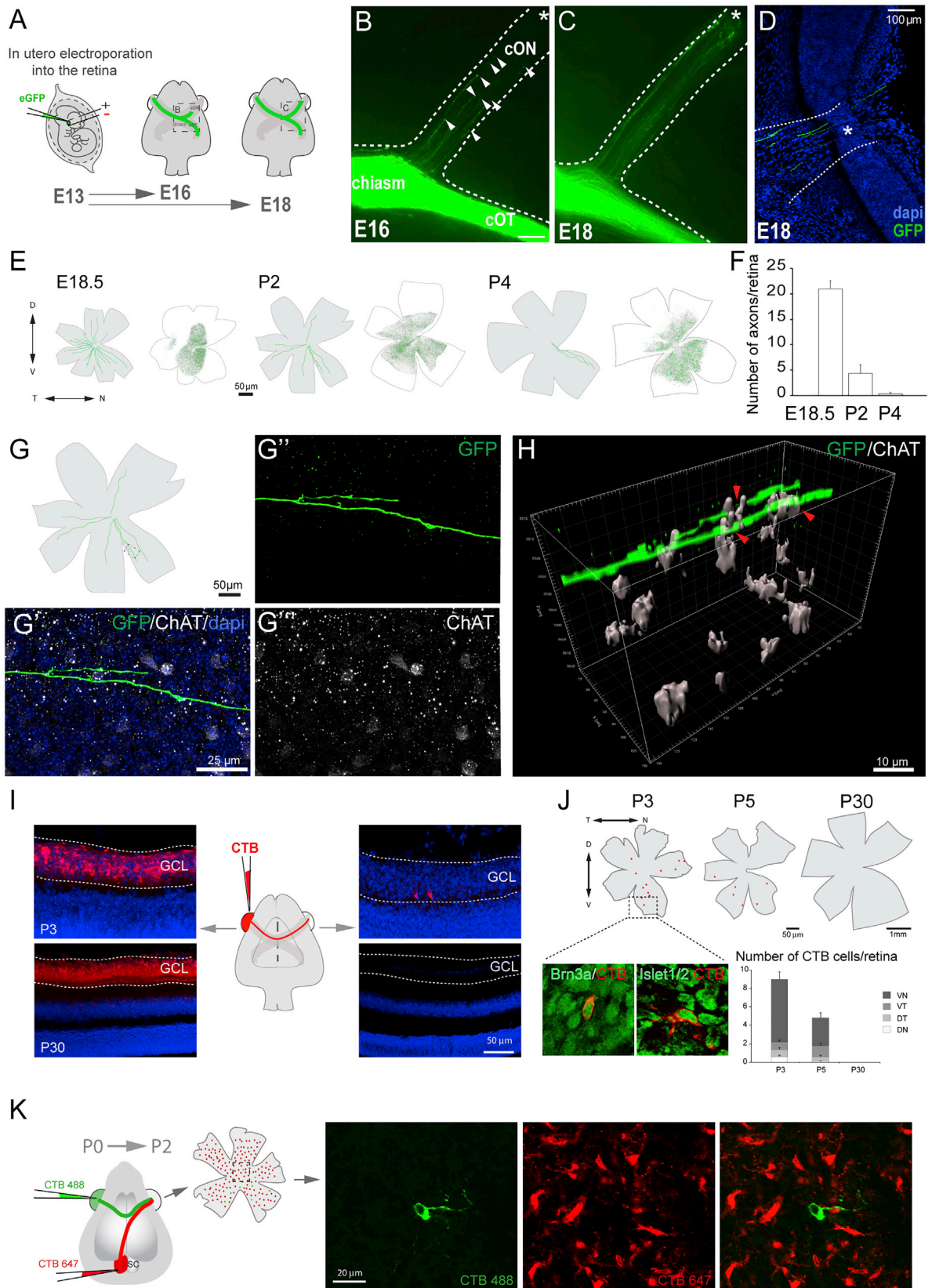
Visual information is perceived by each retina and transmitted to the brain through retinal ganglion cell (RGC) axons. RGC axons extend from each eye via the optic nerves and meet at the ventral diencephalon to form the optic chiasm. Here, axons in all species

cross the midline to join the contralateral tract. In species with stereoscopic vision, a number of RGCs do not cross at the chiasm but project, together with contralateral axons from the other eye, to the superior colliculus (SC) and the lateral geniculate nucleus in a topographical and eye-specific manner. The topographic arrangement at the targets allows the perception of a continuous visual field image on the target [1–4] and is established initially through molecular recognition mediated mainly by Ephs and ephrins, followed by an activity-dependent local refinement of exuberant terminals influenced by electrical activity waves generated spontaneously in the retina before eye opening [5–8].

In addition to the RGC axons that connect each retina with targets in the brain, a direct connection between both retinas (R-R projection) has been reported in different vertebrates [6, 9–19]. However, R-R axons have been detected in only very low numbers and seem to be largely absent in adult animals [11, 14, 15]. As a consequence, they have been considered artifacts of the axonal tracing method or a consequence of axonal projection errors during development. The recent visualization of a subset of calcium waves traveling from the retina to the SC in a simultaneous bilateral manner raised the hypothesis that interactions brought about by an R-R projection could be responsible for synchronizing retinal waves [6]. This idea is further supported by recent results demonstrating that enucleation of one eye alters retinal waves in the remaining eye [20].

Here, we demonstrate unequivocally the existence of an R-R projection that emerges predominately from the central part of the ventral-nasal retina, a region that transiently expresses the axon guidance receptor *Unc5c*. Loss-of-function experiments revealed that *Unc5c*, a receptor for *Netrin1* that is expressed at the optic chiasm, is required for RGCs to extend their axons into the contralateral optic nerve. Conversely, ectopic expression of *Unc5c* forces axons to join the contralateral optic nerve. In addition, *Zic2*, a transcription factor that specifies ipsilateral RGCs [21], represses *Unc5c* expression in ipsilateral axons, supporting the idea that *Unc5c* needs to be downregulated in RGC axons to facilitate growth into the optic tracts. We also found that retinal expression of *Unc5c* in different species is consistent with a computational model in which R-R projections synchronize retinal spontaneous activity in bilateral species that undergo an





(legend on next page)

important axon refinement process during the maturation of the visual system.

## RESULTS

### Characterization of the R-R Projection in the Mouse Visual System

To characterize the development of the R-R projection in the mouse visual system, embryonic day (E) 13.5 embryos were electroporated in one eye with EGFP-encoding plasmids (CAG-EGFP), and three (E16.5), five (E18.5), seven (postnatal day 2 [P2]), or nine (P4) days later, axon trajectories at the chiasm were analyzed (Figure 1). This labeling method eliminates the possibility of labeling artifacts resulting from transfer between cells. At E16.5, although the majority of EGFP-axons projected to the contralateral optic tract, some axons entered the contralateral optic nerve (Figures 1A and 1B). By E18.5, more EGFP-positive axons were found in the contralateral optic nerve and most had reached the contralateral retina (Figures 1C and 1D).

To visualize the trajectory of EGFP axons in the opposite retina, we analyzed whole-mount retinal preparations from E18.5 embryos electroporated at E13.5 and found EGFP axons all over the retina. The number of labeled axon terminals decreased at P2, and very few were detected at P4 (Figures 1E and 1F). The two main types of neurons located in the RGC layer are RGCs and starburst amacrine cells. Labeling of these cells with antibodies against Brn3b, Tuj1 (Figure S1A) and choline-acetyl-transferase (ChAT), respectively, in retinas containing EGFP-R-R axon terminals revealed that amacrine prolongations embrace R-R axons at several sights (Figures 1G and 1H). These experiments confirm the existence of a subpopulation of retinal neurons whose axons reach the opposite retina at perinatal stages and progressively vanish during the first postnatal week. Although further work is required to determine whether R-R axons directly contact starburst amacrine cells, our findings support the hypothesis that these two types of neurons could establish some type of communication.

Next, we mapped the retinal location of R-R neurons. We monocularly injected the retrograde tracer cholera toxin subunit B (CTB)-Alexa-Fluor-594 in newborn mice at several

postnatal stages and analyzed the opposite retina 2 days later (Figure 1I). At P3–P5, retrogradely labeled cells were found into the RGC layer (Figure 1I), were positive for RGC markers (Brn3a and Isl1/2), and located predominately in the ventro-nasal retina (Figure 1J). By P30, no retrogradely labeled cells were found. In an attempt to label a larger number of R-R cells, we injected AAV5-RFP viruses [22] into the eye of E13.5 mouse embryos and analyzed the opposite retina postnatally. We found more cells retrogradely labeled than using CTB, and again, most of them were detected in the ventro-nasal quadrant (Figure S1B). Because the number of retrogradely labeled cells appears to depend on the technique and the timing of injection, it was not possible to quantify the total number of R-R cells. Nevertheless, these experiments demonstrate that R-R RGCs are mainly located in the ventro-nasal region of the retina.

To determine whether R-R axons are collateral branches of RGCs that project to visual targets in the brain, newborn mice were injected with CTB-488 and CTB-647 in the eye and the ipsilateral superior colliculus, respectively. The retina contralateral to the injections side was analyzed 2 days later. None of the CTB-488 cells analyzed were positive for CTB-647 (25 CTB-488 cells from three different pups; Figure 1K). Together with previous studies reporting that retrograde labeling from the eye and the thalamus do not yield double-labeled cells in the retina [23, 24], these results demonstrate that R-R cells are not collateral branches of brain-projecting RGCs.

### Netrin1 Is Expressed in the Ventral Diencephalon at the Time that RGC Axons Transverse the Chiasmatic Region

In contrast to all the other RGC axons, R-R axons do not grow into the ventral region of the optic chiasm. Possible explanations for this behavior include the expression of attractive guidance cues from the contralateral optic nerve and/or repulsive signals at the ventral diencephalon. Among the guidance cues known to be expressed in the ventral diencephalon, Netrin1 has an expression pattern compatible with a putative function as a repellent for R-R RGC axons [25]. *In situ* hybridization on coronal and horizontal sections during the period when RGC axons are navigating through the optic chiasm (E12.5–E14.5) confirmed that *Netrin1* is expressed ventrally in the chiasm at E12.5 and

#### Figure 1. Characterization of Retino-retinal Cells in Mice

(A) Labeled axons from embryos monocularly electroporated with EGFP-encoding plasmids at E13.5 were analyzed at E16.5 or E18.5.

(B–D) At E16.5, EGFP-labeled axons are present within the contralateral optic nerve (cON) (arrowheads, B) and by E18.5 have reached the contralateral optic disc (asterisk, C and D).

(E) Targeted cells (green dots) in retinas electroporated at E13.5 (white flat-mounted retinas) and tracings of EGFP-labeled axons in the contralateral retina (gray flat-mounted retinas) at E18.5–P4.

(F) Mean ( $\pm$  SEM) number of R-R axons in E18.5–P4 retinas after electroporation of the opposite eye at E13.5. These numbers do not represent the total number of R-R neurons, as not all cells are targeted by electroporation.

(G) Diagram of a P2 retina containing R-R axons labeled from the opposite eye. (G'–G''') Image of boxed area in (G) showing an EGFP R-R axon and starburst amacrine cells labeled with ChAT antibodies.

(H) 3D reconstruction of z-projection with a z-step of 1.5  $\mu$ m captured from boxed region in (G) showing ChAT<sup>+</sup> cells embracing the axon terminal (red arrows).

(I) Middle: diagram of monocular injection of CTB. Left: retinal sections of injected P3 and P30 mice injected with CTB 2 days earlier are shown. Right: retinal sections of contralateral retinas from same animals are shown. Note two retrogradely labeled cells in the RGC layer at P3.

(J) Top: diagrams of whole-mount retinas retrogradely labeled with CTB at P3, P5, or P30. Boxed region of P3 retina shows retrogradely labeled cells (red) combined with antibody staining for Brn3a or Isl1/2 (green). Graph shows mean ( $\pm$  SEM) number of labeled cells/retina quadrant. At perinatal stages, most CTB-positive cells are in the ventral quadrants (ventronasal [VN] and ventrotemporal [VT]). At P30, no CTB cells were found.

(K) CTB-488 (green) and CTB-647 (red) were injected in the retina and the ipsilateral superior colliculus (SC), respectively, of newborn mice. The opposite whole-mounted retina was analyzed 2 days later. Right: images from the boxed area show a representative CTB-488 cell negative for CTB-647.

Error bars indicate  $\pm$  SEM.

See also Figure S1.

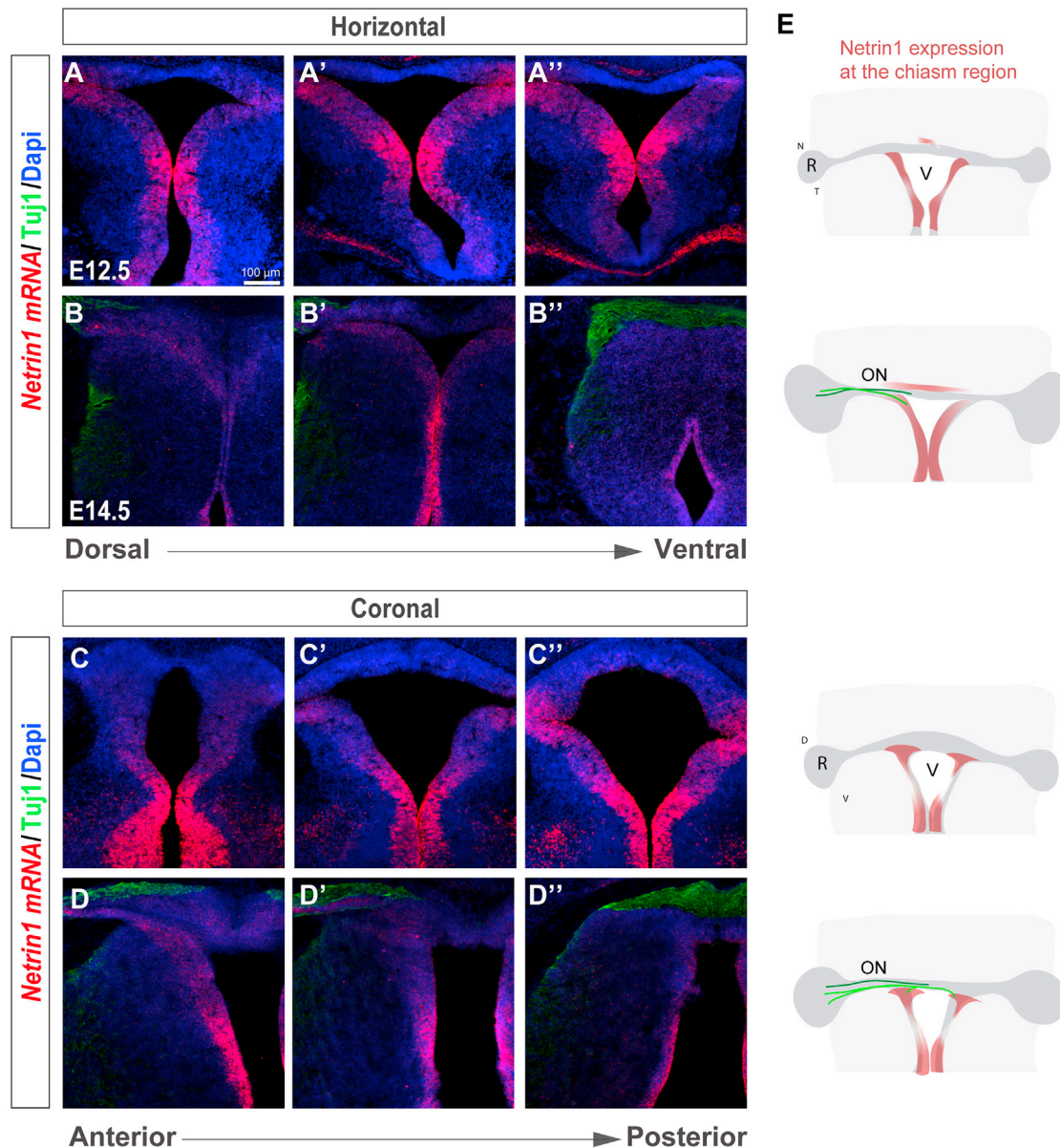


### Figure 2. *Netrin1* Is Expressed at the Developing Ventral Chiasm

(A–D) Horizontal (A–B'') and coronal (C–D'') serial sections of E12.5 (A–A'' and C–C'') and E14.5 (B–B'' and D–D'') embryos at the level of the optic chiasm region stained by *ISH* for *Netrin1* (red) combined with immunofluorescence for Tuj1 (green) to label retinal axons.

(E) Diagram summarizing the spatiotemporal expression of *Netrin1* at the optic chiasm (red). RGC axons projecting to the brain (light green) or to the opposite optic nerve (dark green) are also represented. At E12.5, when RGC axons have not yet arrived at the chiasm, *Netrin1* mRNA is expressed predominately in two patches on both sides of the ventral diencephalon. At E14.5, when axons are at the chiasm region, *Netrin1* mRNA surrounds the optic tracts.

detected strongly at the level of the future optic tracts (Figure 2). At E14.5, *Netrin1* continues to be expressed at the chiasm region and surrounds RGC axons at their most ventral aspect. Thus, the expression of *Netrin1* mRNA is consistent with a role in preventing R-R RGC axons from entering the prospective optic tracts and growing to the brain.

### *Unc5c* Is Expressed in a Subpopulation of Ventral RGCs

*Netrin1* acts through two types of receptors: deleted in colorectal cancer (Dcc) or its homolog Neogenin and *Unc5* [26–31], but only

*Unc5* receptors mediate repulsion [27, 32–34]. The expression patterns in the developing mouse retina of three of the four mammalian *Unc5c* homologs (*Unc5a*, *Unc5b*, and *Unc5d*) have been reported, and none show a pattern consistent with a putative role in the guidance of R-R projections [35]. We therefore analyzed the expression of the remaining family member, *Unc5c*, which has not been reported previously. Using *in situ* hybridization, *Unc5c* was not detected in the retina at E13.5 but by E14.5 was expressed specifically in the ventral region (Figures 3A and 3B). Immunostaining for Brn3a confirmed that *Unc5c*

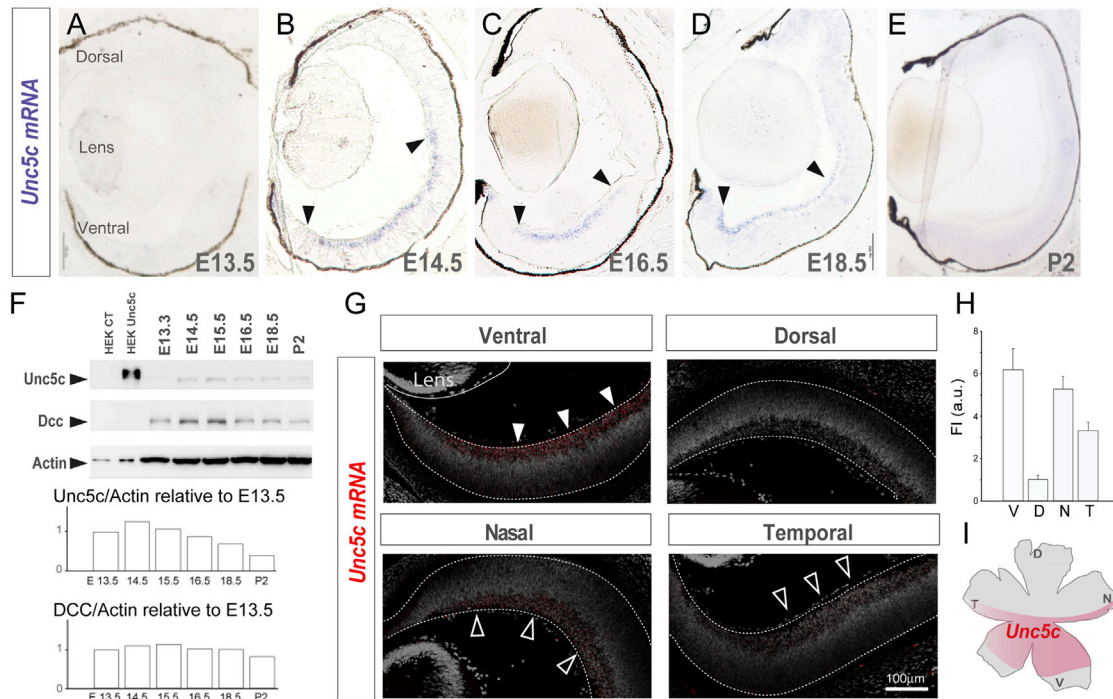


### Figure 3. *Unc5c* Is Expressed in Ventral-Central Retina

(A–E) *In situ* hybridization (ISH) for *Unc5c* in coronal retinal sections at E13.5 (A), E14.5 (B), E16.5 (C), E18.5 (D), and P2 (E) mice.

(F) Immunoblot detection of *Unc5c* and *Dcc* in control (CT) HEK cells and HEK transfected with *Unc5c* encoding plasmids and in E13.5–P2 retinal lysates.  $\beta$ -actin was used as a loading control. Graphs show levels of *Unc5c* and *Dcc* normalized to actin levels. Peak of *Unc5c* expression is at E14.5.

(G) Representative images of *Unc5c* expression (red) in coronal (upper) and horizontal (bottom) retinal sections from E16.5 mouse embryos stained with DAPI (gray).

(H) Mean ( $\pm$  SEM) fluorescent intensity of *Unc5c* in each quadrant of E16.5 retinas.

(I) Diagram of a whole-mounted retina summarizing the expression of *Unc5c* (red).

Error bars indicate  $\pm$  SEM.

See also Figure S2.

mRNA is expressed in the RGC layer (Figure S2A). Expression of both *Unc5c* mRNA and protein was maintained in ventral retina from E14.5 to E18.5 but switched off after birth (Figures 3A–3F). *In situ* hybridization on coronal and horizontal retinal sections confirmed that *Unc5c* is highly expressed in ventral areas and weakly in the dorsal retina. Furthermore, *Unc5c* is detected at higher levels in the nasal than in the temporal quadrant (Figures 3G and 3H). This expression pattern contrasted with that of *Dcc*, which was expressed in RGCs in all retinal regions [25] (Figure S2B). Importantly, the spatial-temporal expression pattern of *Unc5c* mRNA coincides with the location of R-R RGCs in the retina and with the timing of RGCs extending their axons across the optic chiasm. Together with the expression of *Netrin1* at the ventral diencephalon, this expression pattern of *Unc5c* (Figure 3I) strongly suggested an instructive role for *Unc5c* in the development of R-R projections.

### *Unc5c* Is Required for the Formation of the R-R Projection

To elucidate whether *Unc5c* is involved in the development of the R-R pathway, we performed *in vivo* loss-of-function experiments. Labeling of all axons from one eye of E17.5 *Unc5c*-knockout embryos (*Unc5c*<sup>-/-</sup>) and control (*Unc5c*<sup>+/+</sup>) lit-

termates with the lipophilic tracer Dil revealed a clear reduction in the labeling of the contralateral optic nerve in *Unc5c*<sup>-/-</sup> embryos compared with the controls (*Unc5c*<sup>+/+</sup>; Figures 4A–4D). This finding supports the idea that *Unc5c* is essential for the formation of the R-R projection. Retrograde tracing by depositing a Dil crystal in one optic nerve and analyzing the opposite retina resulted in many labeled RGCs in the retinas of E17.5 *Unc5c*<sup>+/+</sup> embryos but very few in *Unc5c*<sup>-/-</sup> littermates (Figures 4E–4H).

To confirm these results, and determine the cell-autonomous function of *Unc5c* in guiding the R-R projection, we carried out additional loss-of-function experiments by specifically downregulating *Unc5c* in RGCs using short hairpin RNAs (shRNAs). Plasmids encoding *Unc5c* shRNA or control scrambled shRNA were monocularly electroporated in the central retina of E13.5 embryos together with EGFP-encoding reporter plasmids and the axons from targeted RGCs analyzed at E16.5 or E18.5. The downregulation of *Unc5c* mRNA in retinas electroporated with *Unc5c* shRNAs confirmed the efficiency of these shRNAs (Figure S3). As expected, in control embryos, most axons crossed the midline and projected into the contralateral optic tract and a small proportion extended into the contralateral optic nerve (Figures 4I and 4I'). However, embryos electroporated with

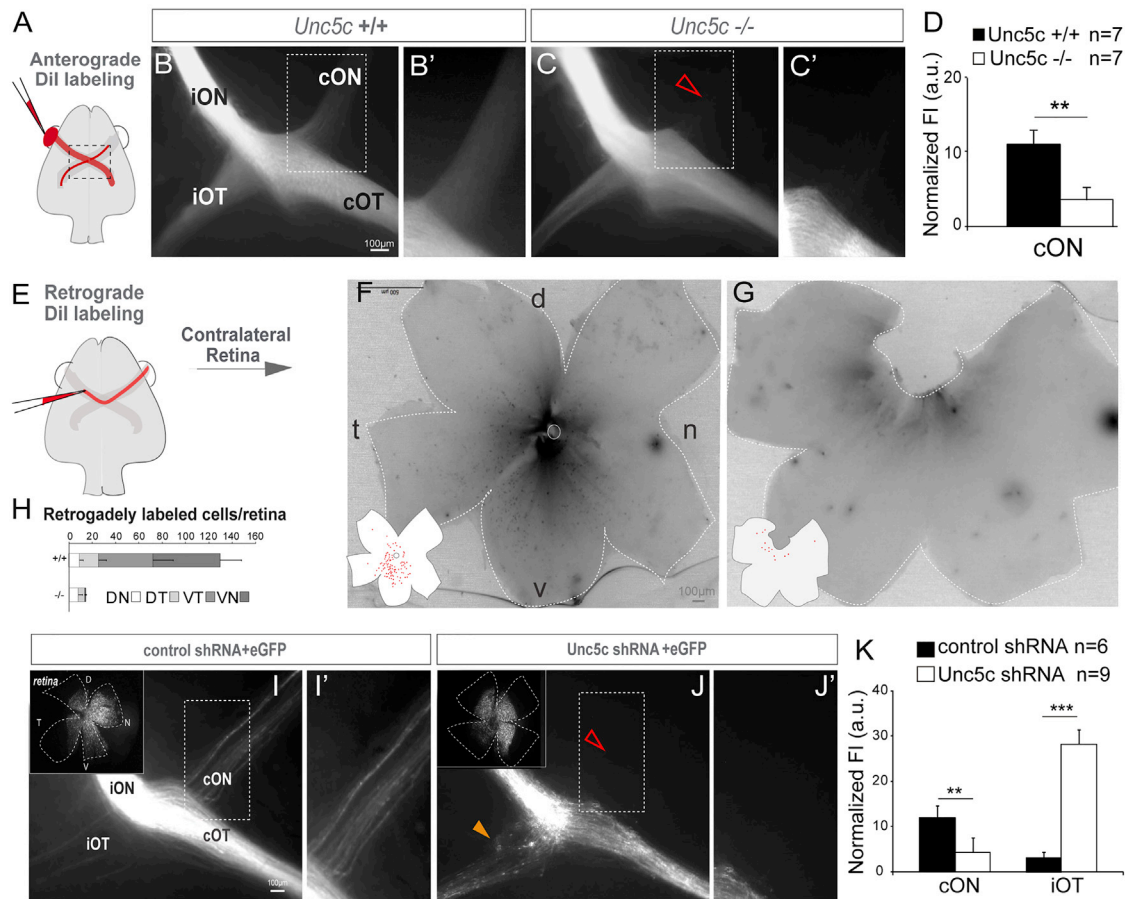


#### Figure 4. *Unc5c* Is Necessary for Establishment of the Retino-retinal Projection

(A–C) Dil was placed into one eye and the labeled axons viewed at the chiasm (A). (B and C) Dil-labeled E17.5 *Unc5c*<sup>+/+</sup> and *Unc5c*<sup>-/-</sup> embryos. The fluorescence intensity in the contralateral optic nerve of the *Unc5c*<sup>-/-</sup> embryo is decreased compared with the control littermate (arrowhead). (B' and C') Higher magnification of the boxed regions in (B) and (C). (D) Mean ( $\pm$  SEM) normalized fluorescence intensity (FI) in the contralateral optic nerve of E17.5 *Unc5c*<sup>-/-</sup> and wild-type embryos monocularly injected with Dil. (E–G) Dil was applied to one optic nerve and the opposite retina analyzed (E). (F and G) Whole-mounted retinas from E17.5 *Unc5c*<sup>+/+</sup> and *Unc5c*<sup>-/-</sup> embryos retrogradely labeled with Dil. Inserts: tracings of the labeled cells are shown. (H) Mean ( $\pm$  SEM) number of retrogradely labeled cells in each quadrant of E17.5 wild-type and *Unc5c* mutant retinas. (I and J) E16.5 embryos electroporated at E13.5 with control or *Unc5c* shRNAs plus EGFP-encoding plasmids. Insert: corresponding whole-mounted electroporated retina is shown. EGFP-positive axons were present in the contralateral optic nerve of control (I and I'), but not *Unc5c* shRNA electroporated, embryos (open arrowhead, J and J'). *Unc5c* electroporated embryos also displayed an ectopic ipsilateral projection (orange arrowhead). (K) Mean ( $\pm$  SEM) normalized fluorescence intensity in the contralateral optic nerve and ipsilateral optic tract of E16.5 embryos electroporated at E13.5 with *Unc5c* shRNA or control shRNA.

cON, contralateral optic nerve; cOT, contralateral optic tract; D, dorsal; iON, ipsilateral optic nerve; iOT, ipsilateral optic tract; N, nasal; T, temporal; V, ventral. Error bars indicate  $\pm$  SEM. (\*\* $p < 0.01$ , \*\*\* $p < 0.001$ , Student's unpaired  $t$  test). See also Figure S3.

*Unc5c* shRNAs showed a dramatic reduction in the number of EGFP axons projecting into the contralateral optic nerve (Figures 4J and 4J'). In addition, a number of labeled axons projected to the ipsilateral optic tract of *Unc5c* shRNA-electroporated embryos (Figures 4I–4K), a phenotype that was not detected in Dil-labeled *Unc5c*<sup>-/-</sup> embryos likely because the endogenous ipsilateral projection masked those R–R axons that changed their trajectories to project ventrally. This unexpected result suggests that *Unc5c*-deficient axons are not repelled away from the ventral diencephalon and, consequently, enter the optic tracts.

#### *Unc5c* Is Not Expressed in Ipsilaterally Projecting RGCs

In retinal sections, *Unc5c* appeared to be consistently excluded from the most peripheral region of the ventral retina (Figures 3C and 3G), which is the location of the RGCs that project ipsilaterally and express the transcription factor *Zic2* [21]. *In situ* hybridization for *Unc5c* combined with immunostaining for *Zic2* in E16.5 retinal sections demonstrated that *Unc5c* and *Zic2* are expressed in mutually exclusive patterns (Figure 5A). In addition, *in situ* hybridization for *Unc5c* in *Zic2*-knockdown embryos (*Zic2*<sup>kd/kd</sup>) revealed that *Unc5c* expression expanded into the peripheral ventro-temporal territory (Figure 5B), the area where *Zic2* is normally

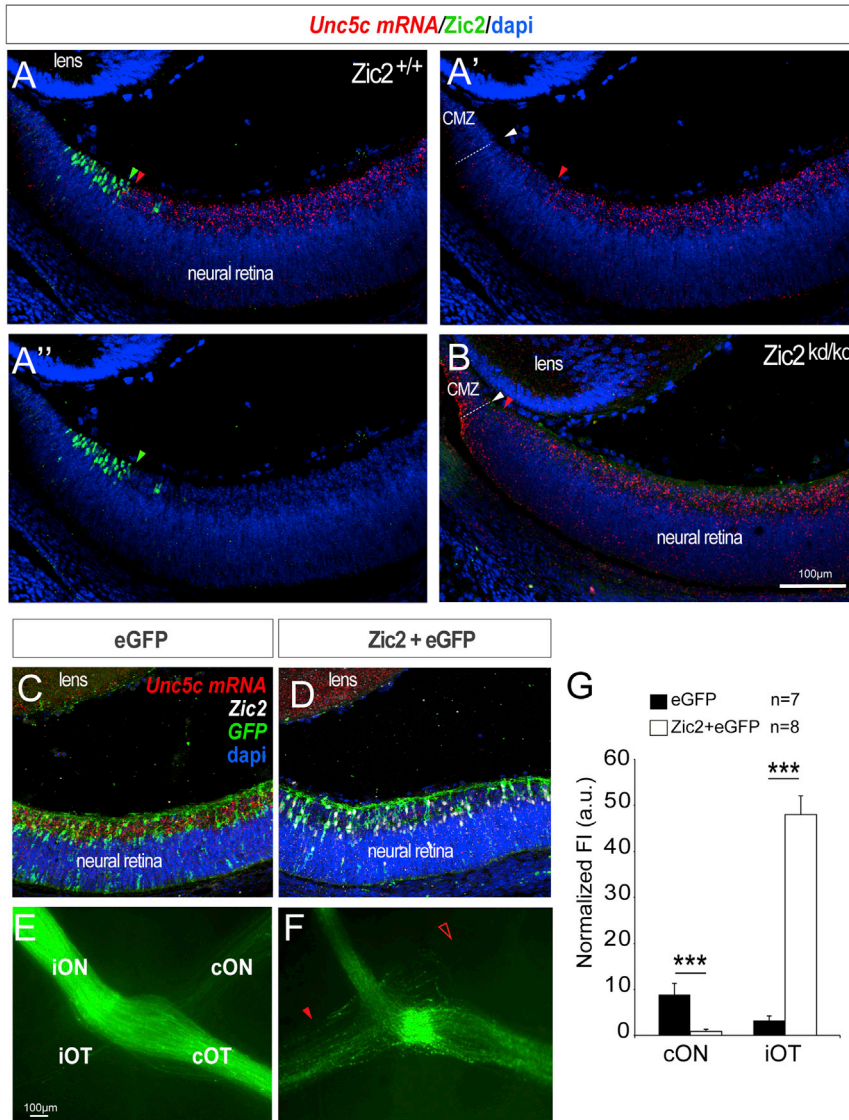


**Figure 5. Ipsilateral RGCs Do Not Express Unc5c**

(A–A'') ISH for *Unc5c* (red) in an E16.5 retinal section shown as a single channel (A') or in combination with immunohistochemistry for Zic2 (green, A and A''). Red arrowheads indicate peripheral limit of *Unc5c* expression, green arrowheads central limit of Zic2 expression, and white arrowhead the region where the neural retina meets the ciliary margin zone (CMZ).

(B) ISH for *Unc5c* (red) combined with immunohistochemistry for Zic2 in Zic2 mutant embryos. Red arrowhead marks the most peripheral limit of *Unc5c* mRNA expression and white arrowhead the region where the neural retina meets the CMZ.

(C and D) ISH for *Unc5c* (red) in retinal sections electroporated with EGFP-encoding (C) or Zic2/EGFP-encoding (D) plasmids. *Unc5c* mRNA expression is reduced after ectopic expression of Zic2.

(E and F) Optic chiasm from E16.5 embryos electroporated with plasmids encoding Zic2/EGFP (F) or EGFP alone (E). Red arrowhead indicates the ectopic ipsilateral projection in embryos electroporated with Zic2 and empty arrowhead the reduced number of EGFP-labeled axons in the contralateral optic nerve of Zic2 electroporated embryos compared to the control.

(G) Mean ( $\pm$  SEM) normalized fluorescence intensity in the contralateral optic nerve and the ipsilateral optic tract of E16.5 embryos electroporated with plasmids encoding Zic2/EGFP or EGFP alone.

Error bars indicate  $\pm$  SEM. (\*\* $p < 0.01$ , \*\*\* $p < 0.001$ , Student's unpaired t test).

expressed [21], suggesting that Zic2 represses *Unc5c* expression. Accordingly, ectopic electroporation of Zic2 into the retina of E13.5 embryos led to downregulation of *Unc5c* (Figures 5C and 5D). Furthermore, axons from RGCs that ectopically express Zic2 never projected into the contralateral optic nerve (Figures 5E–5G). Altogether, these results suggest that Zic2 represses the expression of *Unc5c* in the ventro-temporal retina, making ipsilateral axons insensitive to repulsive signaling from the ventral diencephalon, enabling projection to ipsilateral targets.

#### Unc5c Is Sufficient to Guide Retinal Axons to the Contralateral Retina

We next asked whether *Unc5c* is sufficient to guide RGC axons to the contralateral retina. Plasmids encoding *Unc5c* (CAG-*Unc5c*) together with CAG-EGFP plasmids, or CAG-EGFP plasmids alone, were electroporated *in utero* into the retinas of E13.5 mouse embryos, and 3 (E16.5) or 5 (E18.5) days later, the projection phenotype of the targeted RGCs was analyzed (Figure 6A). As in

previous experiments, a small proportion of control EGFP axons entered the contralateral optic nerve (more at E18.5 than at E16.5; Figures 6B and 6D). In embryos electroporated with *Unc5c*-encoding plasmids, fewer EGFP axons reached the chiasm region compared with controls. This may occur because some axons ectopically expressing *Unc5c* misproject intraretinally (Figure S4), likely as a consequence of Netrin1 expression at the optic disc [36] (Figures S4C and S4C'). However, most *Unc5c*-misexpressing axons were still able to exit the retina by passing through the ring of Netrin1 expression at the optic disc (Figures S4D and S4D'). Importantly, a large percentage of the *Unc5c*-misexpressing axons that reached the optic chiasm grew into the contralateral optic nerve (Figures 6C and 6E), demonstrating that *Unc5c* is sufficient to redirect RGC axons to the contralateral retina. These gain-of-function experiments demonstrate that *Unc5c*-expressing axons are able to transverse the optic disc, despite Netrin1 expression in this region, and that *Unc5c* is sufficient to redirect axons to the contralateral optic nerve.

#### The R-R Projection May Synchronize Retinal Waves to Modulate Bilateral Alignment of Topographic Visual Maps

Our data confirm the existence of an R-R projection and identify guidance mechanisms by which this connection is established.



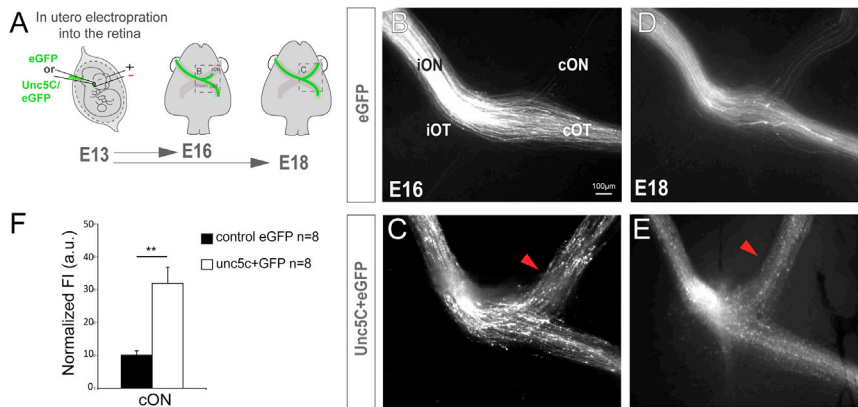


### Figure 6. *Unc5c* Is Sufficient to Guide RGC Axons into the Opposite Optic Nerve

(A) EGFP or *Unc5c*/GFP-encoding plasmids were electroporated into one eye of E13.5 embryos and axons growing into the opposite optic nerve analyzed at E16.5 or E18.5.

(B–E) E16.5 (B and C) and E18.5 (D and E) embryos electroporated with *Unc5c*-encoding plasmids (C and E) display an increase in the number of R-R axons (arrowheads) compared to age-matched controls (B and D).

(F) Mean ( $\pm$  SEM) normalized fluorescence intensity in the cON of E16.5 embryos after electroporation of EGFP or *Unc5c*/GFP-encoding plasmids.

Error bars indicate  $\pm$  SEM. (\*\*\*)  $p < 0.001$ , Student's unpaired t test).

See also Figure S4.

However, although it has been suggested that an R-R projection may help synchronize retinal waves, its specific function remains unknown. To shed some light on this question, we used a simplified version of the classical self-organizing map (SOM) model [37–39]. In the previously proposed SOM model, neighboring neurons compete through lateral interactions to develop into a spatially organized “topographic map.” Although this powerful self-organizing principle can produce a reasonable local distribution of receptive fields, it is necessary to lower the levels of randomness in order to achieve a global order that characterizes the correct orientation of the retinotopic map. This can be accomplished either by introducing some initial order in the early connectivity weights between neurons of the pre- and postsynaptic layer or by structuring the input that the postsynaptic layer receives (see STAR Methods and Figures S5 and S6 for additional details on the mathematical model). In the model proposed here, when the sizes of the pre- (retina) and postsynaptic (SC or tectum) tissues are similar (low  $\sigma$ -molecular values), a congruent map may be established by using a symmetric gradient of molecular guidance cues, one that determines a point-to-point mapping with adequate precision (Figures 7A, S5, and S6). However, when the size of the target tissue is larger than that of the retina (high  $\sigma$ -molecular values), the final map cannot be established with only a simple molecular gradient because errors in topology and folding accumulate. In this latter case, the proper layout of the bilateral retinotopic map critically depends on the synchronization of activity in both maps, particularly in the form of coordinated waves (Figures 7B and S6).

Thus, this mathematical model predicts that the establishment of congruent visual maps in image-forming visual targets may be determined by a point-to-point tagging mechanism in species where the retina and the target tissue have a similar size but that a synchronizing factor must exist in species where RGC axons first create a rough map based on tags and then later undergo a wide refinement process dependent on retinal spontaneous activity. This synchronizing factor may be the R-R connection, and in its absence, topological and unfolding errors increase when the target tissue is bigger than the retina.

The retina and the tectum of lower vertebrates have similar sizes by the time that retinal axons project into this target. Furthermore, it is known that visual mapping in these vertebrates

is established according to a fairly accurate axonal targeting, with only modest further refinement [40] (Figure 7A). In contrast, the target tissue is larger than the retina in amniotes, and the initial collection of arbors reaching the visual targets is loosely organized around the position of the future terminal. A substantial degree of local remodeling then takes place, including the elimination of overshooting portions of RGC axons as well as the removal of inappropriately located branches, to establish the final map [40] (Figure 7B). This local axonal remodeling depends on the action of retinal spontaneous activity [5, 7, 41, 42], and according to our predictive model, both retinas should be connected to assure the synchronization of this activity and promote a bilaterally congruent refinement. Otherwise, axonal refinement would occur independently in each side and thereby create a fractured visual field.

### Retinal Expression of *Unc5c* Correlates with the Existence of an R-R Projection and the Extent of Axonal Refinement at the Visual Targets in Different Species

In zebrafish, retinal axons directly travel to their final locations on the optic tectum, and axon refinement at these visual nuclei is very modest [40]. However, both chickens and mice use an “overshoot and refine” strategy for axons to establish proper connections at the targets in the brain. This occurs upon axons extending into the caudal regions of the tectum in the case of chickens and posterior superior colliculus in the case of mice. To assess a putative correlation between the expression of *Unc5c* in the retina and the existence of an R-R projection and its function in refinement, we analyzed *Unc5c* expression in the developing retinas of zebrafish and chickens. Expression of *Unc5c* was not detected in the developing zebrafish retina at the time that RGC axons grow to reach their targets (36–48 h postfertilization [hpf]; Figures 7C and 7D) [43]. Accordingly, monocular injections of Dil in zebrafish embryos did not reveal R-R projections (Figures 7E and 7E'). In chickens, the existence of a transient R-R projection has been reported previously [17]. In agreement with this, we detected *Unc5c* in the RGC layer of the developing chicken retina (Figure S7). In ferrets, the period of retinal wave-dependent axon refinement is extended for several weeks after birth. We analyzed the expression of *Unc5c* mRNA in ferrets and found it is expressed in the RGC layer of the ventral retina both embryonically (E34) and postnatally (P1)

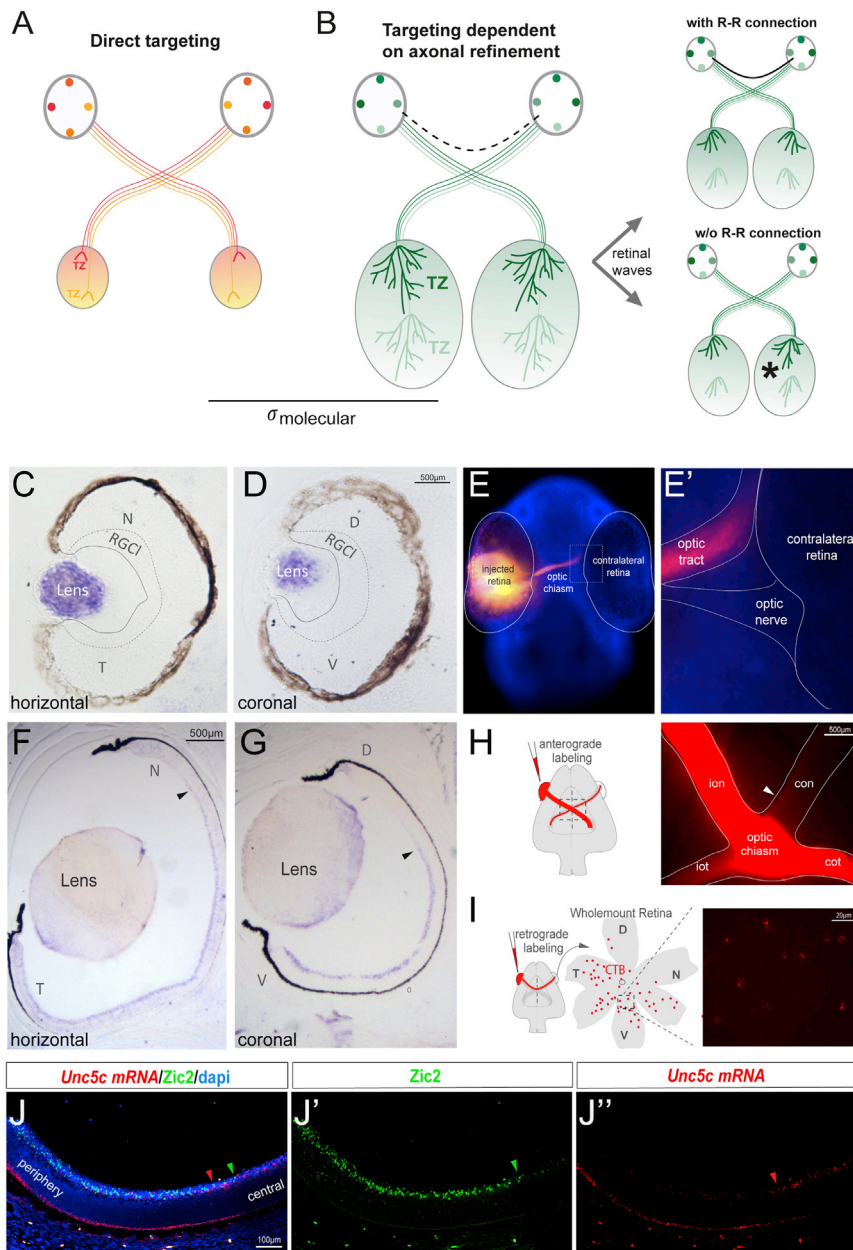


**Figure 7. The R-R Connection through Evolution**

(A) Working model of the function of R-R in different species. In species where the size of the tectum and retina is similar, the establishment of bilaterally congruent maps may rely on point-to-point molecular tagging mechanisms.

(B) In species where the size of the visual target is larger than the retina, map topography relies both on a molecular tagging mechanism and a later refinement process, dependent on waves of spontaneous activity. The presence of an R-R connection may enable the synchronization of retinal waves from each eye, driving symmetrical refinement in both hemispheres.

(C and D) ISH for *Unc5c* in horizontal (C) and coronal (D) sections of the zebrafish retina revealed no expression of *Unc5c*.

(E and E') A 36- to 48-h post fertilization (hpf) zebrafish embryo stained with DAPI and monocularly injected with Dil shows no retinal axons entering into the contralateral retina.

(F and G) ISH for *Unc5c* mRNA in horizontal (F) and coronal (G) sections from P0 ferret retinas. *Unc5c* mRNA is expressed in the RGC layer of ventral and temporal retina.

(H) Schematic diagram representing monocular Dil anterograde labeling. Optic chiasm of a Dil-labeled P0 ferret is shown. White arrowhead points to the axons into the contralateral optic nerve.

(I) Schematic diagram representing retrograde CTB-labeling. CTB injection was performed at P1, and labeled RGCs were visualized by red fluorescence in whole-mount retinas 1 day later.

(J–J'') ISH for *Unc5c* mRNA and immunohistochemistry for *Zic2* in a coronal retinal section from an E34.5 ferret embryo counterstained with DAPI. Red arrowheads mark the most peripheral limit of *Unc5c* mRNA expression and green arrowheads the central limit of *Zic2* expression. *Zic2* and *Unc5c* mRNA expression is mostly complementary.

CTB, cholera toxin subunit B-Alexa594; RGCi, retinal ganglion cell layer. See also Figures S5, S6, and S7 and Table S1.

(data not shown; Figures 7F and 7G). An R-R projection has not been reported previously in ferrets, and to investigate whether they have it, we monocularly injected Dil into a newborn ferret and followed the traced axons. High fluorescence intensity was detected in the contralateral optic nerve, indicating the presence of axons projecting to the opposite retina (Figure 7H). Retrograde labeling by CTB injection into one eye of P1 ferrets demonstrated the existence of R-R neurons in the ventral retina matching the expression of *Unc5c*, with the extent of these neurons being greater than in mice (Figure 7I). Moreover, as in mice, the expression pattern of *Zic2* in the developing retina was complementary to *Unc5c* expression in ferret (Figure 7J). These results in mouse, zebrafish, chick, and ferret strongly support a conserved evolutionary role for the *Zic2*-*Unc5c*-Netrin1 axis in regulating the

formation of the R-R projection, which may be essential for the correct functioning of the visual system in amniotes.

## DISCUSSION

The existence of an R-R projection that connects both eyes has been a controversial issue for some time. Here, monocular electroporation of EGFP-reporter plasmids during embryonic stages definitively demonstrates the existence of an R-R projection that is established during embryogenesis and early postnatal stages. The formation of this visual pathway depends on *Unc5c*-mediated signaling in RGC axons and, likely, on its ligand Netrin1, which is expressed at the ventral aspect of the developing diencephalon. Species without R-R projections (e.g., zebrafish) do not express

Unc5c in the retina, whereas species with R-R-projecting neurons (e.g., mouse, chick, and ferret) express Unc5c in the RGC layer when retinal axons are passing through the optic chiasm region. These observations uncover a conserved role for Unc5c in controlling the formation of R-R projections in the developing retina and indicate a positive selection for this mechanism through evolution. Together with functional experiments and a computational model, our results suggest that the R-R projection play an important role in the congruency of visual maps in species that undergo intensive retinal wave-dependent axon refinement during development.

### Unc5c/Netrin1 Repulsive Signaling as a Candidate to Direct R-R Axons to the Contralateral Optic Nerve

Although our data are consistent with a repulsive role for Netrin/Unc5c signaling in directing navigation of R-R axons at the chiasm, further experiments are crucial to confirm this idea. Conditional removal of Netrin1 from the chiasm region would be necessary to uncover the role of Netrin1 in the formation of the R-R. Also, because (1) EphB2 is expressed in the ventral retina [44], (2) Netrin and ephrins play a synergistic effect in axons expressing EphBs and Unc5 receptors [45], and (3) ephrinB2 is expressed at the midline [46], further work is needed to establish whether EphB2 and/or ephrinB2 is involved in modulating Unc5c-mediated guidance of R-R axons.

### The Function of the R-R Projection in Different Species

A simple, single-retina SOM model, when stimulated randomly with a uniform distribution, can readily generate postsynaptic maps that reproduce the geometry of the presynaptic layer (Figures 7 and S6). These maps, however, are rarely oriented correctly because there are four different ways in which two square grids can be oriented relative to each other, and only one of these orientations is topologically correct. Thus, the probability of generating the correct map between the retina and its targets in the brain is only 1/24 (~4%). Furthermore, if we consider that two independent retinas must be correctly laid out at the same time, the probability drops even further to  $(1/24)^2$  (~0.02%). Our modeling results show that the concurrent contribution of the gradients of molecular guidance cues and the bilateral coordination of retinal activity afforded by an R-R projection helps avoid such an orientation error.

Retinal waves have been proposed as an evolutionary adaptation in animals with extended periods of visual development [47] to help set a functional visual system before eye opening. Coordinated waves of spontaneous activity occur in the visual system before the onset of visual experience in all amniote species that have been examined to date (turtles, chicks, rats, mice, ferrets, cats, and monkeys) [7, 48]. In mice, the number of R-R axons seems to peak at perinatal stages, a period that coincides with the cholinergic phase of spontaneous retinal activity (see [49] for a recent review). Compared with mice, ferrets experience an extended period of spontaneous retinal waves that last several weeks after birth [5, 50–52]. Non-amniote vertebrates only have a brief gestational period before the beginning of vision, and as such, the role of spontaneous patterned activity in these species is likely assumed by sensory experience. Interestingly, spontaneous waves have not been found in non-amniotes [47, 53]. Our results demonstrating that ferrets have more R-R axons than mice, and zebrafish lack an R-R projection,

support the hypothesis that, in amniotes, both retinas must be connected to ensure a correct bilateral refinement. The fact that chickens have Unc5c, but not Zic2 [21], also argues that R-R projections emerged during evolution to match axonal refinement in the visual targets at both sides of the brain and suggests that stereoscopic vision, which depends on Zic2-driven ipsilateral projection, emerged on top of this feature. Adams and Horton theorized years ago that spontaneous waves would need to occur simultaneously in both eyes to generate the striking symmetry observed in the global patterns of dominance columns [54]. The results shown here provide an avenue by which spontaneous retinal waves could be synchronized in order to fine-tune bilateral topographic maps and give rise to a congruent visual image in direct visual nuclei, as well as in the visual cortex of animals that have a particularly elaborated visual system.

### STAR★METHODS

Detailed methods are provided in the online version of this paper and include the following:

- KEY RESOURCES TABLE
- CONTACT FOR REAGENT AND RESOURCE SHARING
- EXPERIMENTAL MODEL AND SUBJECT DETAILS
- METHOD DETAILS
  - Plasmids
  - In utero electroporation and Dil tracing
  - CTB injections and adenovirus infection
  - Western Blot
  - *In situ* hybridization and immunohistochemistry
  - Microscopy setup
  - Mathematical Model
- QUANTIFICATION AND STATISTICAL ANALYSIS

### SUPPLEMENTAL INFORMATION

Supplemental Information can be found with this article online at <https://doi.org/10.1016/j.cub.2019.02.052>.

### ACKNOWLEDGMENTS

We thank D. Baeza and M. Herrera for mouse breeding, genotyping and E. Llorens and J. Mullet for technical help in experiments involving ferrets. We also thank A. Barco for discussion and comments on the manuscript. The laboratory of E.H. is funded with the following grants: BFU2016-77605 from the National Grant Research Program; PROMETEO Program [2016/026] from Generalitat Valenciana; PCIN2015-192-C02-02 from ERA-Net Program; and ERC-282329 from the European Research Council. Work in the laboratory of L.M.M. and S.S. was supported by the National Grant Research Program (grant BFU2014-58776), co-financed by the European Regional Development Fund (ERDF). V.M.-B. holds a postdoctoral contract from the Generalitat Valenciana. A.J.V. is the recipient of a FPI fellowship from the National Grant Research Program. We also acknowledge the financial support received from the “Severo Ochoa” Program for Centers of Excellence in R&D (SEV-2013-0317). A.K. was supported by the Canadian Institutes of Health Research operating grants MOP-77556 and MOP-97758, as well as Brain Canada, Canadian Foundation for Innovation, and the W. Garfield Weston Foundation.

### AUTHOR CONTRIBUTIONS

V.M.-B. performed and analyzed most of the experiments. C.V. made the initial observations on the expression of Unc5c in the developing retina and

performed some gain-of-function experiments. Y.C. has performed *in utero* electroporations and axon tracer injections assisted by S.N. R.D. and A.K. provided the *Unc5c* mice. C.d.J. and V.B. provided and performed *in situ* hybridization and immunohistochemistry in ferret embryos; A.J.V., S.S., and L.M.M. generated the computation model. E.H. wrote the original draft and conceived and supervised the study. A.K., V.B., and L.M.M. revised subsequent versions of the manuscript. L.E. helped with experimental design and revisited critically the manuscript for important intellectual content.

## DECLARATION OF INTERESTS

The authors declare no competing interests.

Received: October 4, 2018

Revised: January 4, 2019

Accepted: February 22, 2019

Published: March 21, 2019

## REFERENCES

- Cang, J., Niell, C.M., Liu, X., Pfeifferberger, C., Feldheim, D.A., and Stryker, M.P. (2008). Selective disruption of one Cartesian axis of cortical maps and receptive fields by deficiency in ephrin-As and structured activity. *Neuron* 57, 511–523.
- Godement, P., Salaün, J., and Imbert, M. (1984). Prenatal and postnatal development of retinogeniculate and retinocollicular projections in the mouse. *J. Comp. Neurol.* 230, 552–575.
- Lemke, G., and Reber, M. (2005). Retinotectal mapping: new insights from molecular genetics. *Annu. Rev. Cell Dev. Biol.* 21, 551–580.
- Nakamura, H., and O'Leary, D.D. (1989). Inaccuracies in initial growth and arborization of chick retinotectal axons followed by course corrections and axon remodeling to develop topographic order. *J. Neurosci.* 9, 3776–3795.
- Huberman, A.D., Feller, M.B., and Chapman, B. (2008). Mechanisms underlying development of visual maps and receptive fields. *Annu. Rev. Neurosci.* 31, 479–509.
- Ackman, J.B., Burbridge, T.J., and Crair, M.C. (2012). Retinal waves coordinate patterned activity throughout the developing visual system. *Nature* 490, 219–225.
- Ackman, J.B., and Crair, M.C. (2014). Role of emergent neural activity in visual map development. *Curr. Opin. Neurobiol.* 24, 166–175.
- Erskine, L., and Herrera, E. (2014). Connecting the retina to the brain. *ASN Neuro* 6, 1759091414562107.
- Bohn, R.C., and Stelzner, D.J. (1981). The aberrant retino-retinal projection during optic nerve regeneration in the frog. II. Anterograde labeling with horseradish peroxidase. *J. Comp. Neurol.* 196, 621–632.
- Braekevelt, C.R., Beazley, L.D., Dunlop, S.A., and Darby, J.E. (1986). Numbers of axons in the optic nerve and of retinal ganglion cells during development in the marsupial *Setonix brachyurus*. *Brain Res.* 390, 117–125.
- Bunt, S.M., and Lund, R.D. (1981). Development of a transient retino-retinal pathway in hooded and albino rats. *Brain Res.* 211, 399–404.
- Humphrey, M.F., and Beazley, L.D. (1985). Retinal ganglion cell death during optic nerve regeneration in the frog *Hyla moorei*. *J. Comp. Neurol.* 236, 382–402.
- McLoon, S.C., and Lund, R.D. (1982). Transient retinofugal pathways in the developing chick. *Exp. Brain Res.* 45, 277–284.
- Müller, M., and Holländer, H. (1988). A small population of retinal ganglion cells projecting to the retina of the other eye. An experimental study in the rat and the rabbit. *Exp. Brain Res.* 71, 611–617.
- Nadal-Nicolás, F.M., Valiente-Soriano, F.J., Salinas-Navarro, M., Jiménez-López, M., Vidal-Sanz, M., and Agudo-Barriso, M. (2015). Retino-retinal projection in juvenile and young adult rats and mice. *Exp. Eye Res.* 134, 47–52.
- Tennant, M., Bruce, S.R., and Beazley, L.D. (1993). Survival of ganglion cells which form the retino-retinal projection during optic nerve regeneration in the frog. *Vis. Neurosci.* 10, 681–686.
- Thanos, S. (1999). Genesis, neurotrophin responsiveness, and apoptosis of a pronounced direct connection between the two eyes of the chick embryo: a natural error or a meaningful developmental event? *J. Neurosci.* 19, 3900–3917.
- Tóth, P., and Straznicky, C. (1989). Retino-retinal projections in three anuran species. *Neurosci. Lett.* 104, 43–47.
- Tang, X., Tzekov, R., and Passaglia, C.L. (2016). Retinal cross talk in the mammalian visual system. *J. Neurophysiol.* 115, 3018–3029.
- Failor, S.W., Ng, A., and Cheng, H.J. (2018). Monocular enucleation alters retinal waves in the surviving eye. *Neural Dev.* 13, 4.
- Herrera, E., Brown, L., Aruga, J., Rachel, R.A., Dolan, G., Mikoshiba, K., Brown, S., and Mason, C.A. (2003). *Zic2* patterns binocular vision by specifying the uncrossed retinal projection. *Cell* 114, 545–557.
- Aschauer, D.F., Kreuz, S., and Rumpel, S. (2013). Analysis of transduction efficiency, tropism and axonal transport of AAV serotypes 1, 2, 5, 6, 8 and 9 in the mouse brain. *PLoS ONE* 8, e76310.
- Pratt, T., Conway, C.D., Tian, N.M., Price, D.J., and Mason, J.O. (2006). Heparan sulphation patterns generated by specific heparan sulfotransferase enzymes direct distinct aspects of retinal axon guidance at the optic chiasm. *J. Neurosci.* 26, 6911–6923.
- Pratt, T., Tian, N.M., Simpson, T.I., Mason, J.O., and Price, D.J. (2004). The winged helix transcription factor *Foxg1* facilitates retinal ganglion cell axon crossing of the ventral midline in the mouse. *Development* 131, 3773–3784.
- Deiner, M.S., and Sretavan, D.W. (1999). Altered midline axon pathways and ectopic neurons in the developing hypothalamus of netrin-1- and DCC-deficient mice. *J. Neurosci.* 19, 9900–9912.
- Ackerman, S.L., Kozak, L.P., Przyborski, S.A., Rund, L.A., Boyer, B.B., and Knowles, B.B. (1997). The mouse rostral cerebellar malformation gene encodes an UNC-5-like protein. *Nature* 386, 838–842.
- Hamelin, M., Zhou, Y., Su, M.W., Scott, I.M., and Culotti, J.G. (1993). Expression of the UNC-5 guidance receptor in the touch neurons of *C. elegans* steers their axons dorsally. *Nature* 364, 327–330.
- Hong, K., Hinck, L., Nishiyama, M., Poo, M.M., Tessier-Lavigne, M., and Stein, E. (1999). A ligand-gated association between cytoplasmic domains of UNC5 and DCC family receptors converts netrin-induced growth cone attraction to repulsion. *Cell* 97, 927–941.
- Leonardo, E.D., Hinck, L., Masu, M., Keino-Masu, K., Ackerman, S.L., and Tessier-Lavigne, M. (1997). Vertebrate homologues of *C. elegans* UNC-5 are candidate netrin receptors. *Nature* 386, 833–838.
- Leung-Hagesteijn, C., Spence, A.M., Stern, B.D., Zhou, Y., Su, M.W., Hedgecock, E.M., and Culotti, J.G. (1992). UNC-5, a transmembrane protein with immunoglobulin and thrombospondin type 1 domains, guides cell and pioneer axon migrations in *C. elegans*. *Cell* 71, 289–299.
- Vielmetter, J., Kayyem, J.F., Roman, J.M., and Dreyer, W.J. (1994). Neogenin, an avian cell surface protein expressed during terminal neuronal differentiation, is closely related to the human tumor suppressor molecule deleted in colorectal cancer. *J. Cell Biol.* 127, 2009–2020.
- Colamarino, S.A., and Tessier-Lavigne, M. (1995). The axonal chemoattractant netrin-1 is also a chemorepellent for trochlear motor axons. *Cell* 81, 621–629.
- Fazeli, A., Dickinson, S.L., Hermiston, M.L., Tighe, R.V., Steen, R.G., Small, C.G., Stoeckli, E.T., Keino-Masu, K., Masu, M., Rayburn, H., et al. (1997). Phenotype of mice lacking functional Deleted in colorectal cancer (*Dcc*) gene. *Nature* 386, 796–804.
- Hedgecock, E.M., Culotti, J.G., and Hall, D.H. (1990). The *unc-5*, *unc-6*, and *unc-40* genes guide circumferential migrations of pioneer axons and mesodermal cells on the epidermis in *C. elegans*. *Neuron* 4, 61–85.
- Engelkamp, D. (2002). Cloning of three mouse *Unc5* genes and their expression patterns at mid-gestation. *Mech. Dev.* 118, 191–197.

36. Deiner, M.S., Kennedy, T.E., Fazeli, A., Serafini, T., Tessier-Lavigne, M., and Sretavan, D.W. (1997). Netrin-1 and DCC mediate axon guidance locally at the optic disc: loss of function leads to optic nerve hypoplasia. *Neuron* *19*, 575–589.
37. Kohonen, T. (1982). Self-organized formation of topologically correct feature maps. *Biol. Cybern.* *43*, 59–69.
38. Kohonen, T. (2013). Essentials of the self-organizing map. *Neural Netw.* *37*, 52–65.
39. Willshaw, D.J., von der Malsburg, C., and Longuet-Higgins, H.C. (1976). How patterned neural connections can be set up by self-organization. *Proc. R. Soc. Lond. B. Biol. Sci.* *194*, 431–445.
40. McLaughlin, T., and O’Leary, D.D. (2005). Molecular gradients and development of retinotopic maps. *Annu. Rev. Neurosci.* *28*, 327–355.
41. Erzurumlu, R.S., and Kind, P.C. (2001). Neural activity: sculptor of ‘barrels’ in the neocortex. *Trends Neurosci.* *24*, 589–595.
42. Goodman, C.S., and Shatz, C.J. (1993). Developmental mechanisms that generate precise patterns of neuronal connectivity. *Cell* *72* (Suppl), 77–98.
43. Dingwell, K.S., Holt, C.E., and Harris, W.A. (2000). The multiple decisions made by growth cones of RGCs as they navigate from the retina to the tectum in *Xenopus* embryos. *J. Neurobiol.* *44*, 246–259.
44. Thakar, S., Chenaux, G., and Henkemeyer, M. (2011). Critical roles for EphB and ephrin-B bidirectional signalling in retinocollicular mapping. *Nat. Commun.* *2*, 431.
45. Poliak, S., Morales, D., Croteau, L.P., Krawchuk, D., Palmesino, E., Morton, S., Cloutier, J.F., Charron, F., Dalva, M.B., Ackerman, S.L., et al. (2015). Synergistic integration of Netrin and ephrin axon guidance signals by spinal motor neurons. *eLife* *4*, e10841.
46. Williams, S.E., Mason, C.A., and Herrera, E. (2004). The optic chiasm as a midline choice point. *Curr. Opin. Neurobiol.* *14*, 51–60.
47. Demas, J.A., Payne, H., and Cline, H.T. (2012). Vision drives correlated activity without patterned spontaneous activity in developing *Xenopus* retina. *Dev. Neurobiol.* *72*, 537–546.
48. Wong, R.O. (1999). Retinal waves and visual system development. *Annu. Rev. Neurosci.* *22*, 29–47.
49. Leighton, A.H., and Lohmann, C. (2016). The wiring of developing sensory circuits—from patterned spontaneous activity to synaptic plasticity mechanisms. *Front. Neural Circuits* *10*, 71.
50. Arroyo, D.A., and Feller, M.B. (2016). Spatiotemporal features of retinal waves instruct the wiring of the visual circuitry. *Front. Neural Circuits* *10*, 54.
51. Bennett, J.E., and Bair, W. (2015). Refinement and pattern formation in neural circuits by the interaction of traveling waves with spike-timing dependent plasticity. *PLoS Comput. Biol.* *11*, e1004422.
52. Burgi, P.Y., and Grzywacz, N.M. (1994). Model for the pharmacological basis of spontaneous synchronous activity in developing retinas. *J. Neurosci.* *14*, 7426–7439.
53. Zhang, R.W., Li, X.Q., Kawakami, K., and Du, J.L. (2016). Stereotyped initiation of retinal waves by bipolar cells via presynaptic NMDA autoreceptors. *Nat. Commun.* *7*, 12650.
54. Adams, D.L., and Horton, J.C. (2003). Capricious expression of cortical columns in the primate brain. *Nat. Neurosci.* *6*, 113–114.
55. Marcucci, F., Murcia-Belmonte, V., Wang, Q., Coca, Y., Ferreiro-Galve, S., Kuwajima, T., Khalid, S., Ross, M.E., Mason, C., and Herrera, E. (2016). The ciliary margin zone of the mammalian retina generates retinal ganglion cells. *Cell Rep.* *17*, 3153–3164.
56. Murcia-Belmonte, V., Expósito, G., and Herrera, E. (2017). Time-lapse imaging and cell tracking of migrating cells in slices and flattened telencephalic vesicles. *Curr. Protoc. Neurosci.* *79*, 3.31.1–3.31.12.
57. Murillo, B., Ruiz-Reig, N., Herrera, M., Fairén, A., and Herrera, E. (2015). *Zic2* controls the migration of specific neuronal populations in the developing forebrain. *J. Neurosci.* *35*, 11266–11280.
58. Tiveron, M.C., Beclin, C., Murgan, S., Wild, S., Angelova, A., Marc, J., Coré, N., de Chevigny, A., Herrera, E., Bosio, A., et al. (2017). *Zic*-proteins are repressors of dopaminergic forebrain fate in mice and *C. elegans*. *J. Neurosci.* *37*, 10611–10623.
59. Garcia-Frigola, C., Carreres, M.I., Vegar, C., and Herrera, E. (2007). Gene delivery into mouse retinal ganglion cells by in utero electroporation. *BMC Dev. Biol.* *7*, 103.
60. Hamburger, V., and Hamilton, H.L. (1951). A series of normal stages in the development of the chick embryo. *J. Morphol.* *88*, 49–92.
61. Kimmel, C.B., Ballard, W.W., Kimmel, S.R., Ullmann, B., and Schilling, T.F. (1995). Stages of embryonic development of the zebrafish. *Dev. Dyn.* *203*, 253–310.
62. Scandaglia, M., Benito, E., Morenilla-Palao, C., Fiorenza, A., Del Blanco, B., Coca, Y., Herrera, E., and Barco, A. (2015). Fine-tuned SRF activity controls asymmetrical neuronal outgrowth: implications for cortical migration, neural tissue lamination and circuit assembly. *Sci. Rep.* *5*, 17470.
63. Plump, A.S., Erskine, L., Sabatier, C., Brose, K., Epstein, C.J., Goodman, C.S., Mason, C.A., and Tessier-Lavigne, M. (2002). *Slit1* and *Slit2* cooperate to prevent premature midline crossing of retinal axons in the mouse visual system. *Neuron* *33*, 219–232.
64. Rebsam, A., Petros, T.J., and Mason, C.A. (2009). Switching retinogeniculate axon laterality leads to normal targeting but abnormal eye-specific segregation that is activity dependent. *J. Neurosci.* *29*, 14855–14863.
65. Schaeren-Wiemers, N., and Gerfin-Moser, A. (1993). A single protocol to detect transcripts of various types and expression levels in neural tissue and cultured cells: in situ hybridization using digoxigenin-labelled cRNA probes. *Histochemistry* *100*, 431–440.

## STAR★METHODS

## KEY RESOURCES TABLE

REAGENT or RESOURCE	SOURCE	IDENTIFIER
<b>Antibodies</b>		
Mouse monoclonal antibody anti- $\beta$ -actin (1:10000 for WB)	Sigma-Aldrich	Cat#A5441; RRID:AB_476744
Goat polyclonal antibody anti-DCC (A-20) (1:100 for WB)	Santa Cruz	Cat#sc-6535; RRID:AB_2245770
Rabbit anti-human Unc5c polyclonal antibody (1:500 for WB)	Abcam	Cat#ab91408; RRID:AB_2212873
Chicken polyclonal antibody anti-GFP (1:2000 for IF)	Aves Labs	Cat#GFP-1020; RRID:AB_10000240
Rabbit polyclonal antibody anti-Zic2 (1:1000 for IF)	This lab (previous study [55–58])	N/A
Mouse neuron class III $\beta$ -Tubulin monoclonal antibody (anti-Tuj1) (1:1000 for IF)	Covance	Cat#MMS-435P; RRID:AB_2313773
Rabbit specific beta III tubulin antibody (1:1000 for IF)	Abcam	Cat#ab18207; RRID:AB_444319
Mouse monoclonal antibody anti-Brn3a (1:300 for IF)	Millipore	Cat#MAB1585; RRID:AB_94166
Rabbit polyclonal antibody anti-calbindin D-28k (1:1000 for IF)	Swant	Cat#CB38; RRID:AB_2721225
Goat polyclonal antibody anti-ChAT (1:100 for IF)	Millipore	Cat#AB144P; RRID:AB_2079751
Mouse monoclonal antibody anti-Isl1/2 (39.4D5) (1:500 for IF)	Hybridoma Bank	Cat#39.4D5; RRID:AB_2314683
<b>Bacterial and Virus Strains</b>		
pAAV-CAG-tdTomato	Addgene	Cat#59462-AAV5
<b>Chemicals, Peptides, and Recombinant Proteins</b>		
Cholera toxin B subunit (CTB)-Alexa 594	ThermoFisher	Cat#C22842
Cholera toxin B subunit (CTB)-Alexa 488	ThermoFisher	Cat#C34775
Cholera toxin B subunit (CTB)-Alexa 647	ThermoFisher	Cat#C34778
TEMED	Sigma-Aldrich	Cat#T9281
Acrylamide solution	Sigma-Aldrich	Cat#A4058
Lipofectamine 2000	Thermo Fisher Scientific	Cat#11668019
Penicillin/Streptomycin	Sigma-Aldrich	Cat#P0781
cOmplete Mini EDTA-free protease inhibitor cocktail tablets	Sigma-Aldrich	Cat#11836170001
IGEPAL CA-630	Sigma-Aldrich	Cat#I8896
Laemliis buffer	Sigma-Aldrich	Cat#S3401
Protein Assay Dye Reagent Concentrate	Bio-Rad	Cat#5000006
Dimethylsulphoxide (DMSO)	Sigma-Aldrich	Cat#D2650
Paraformaldehyde	Sigma-Aldrich	Cat#30525-89-4
<b>Experimental Models: Cell Lines</b>		
HEK293 cells	ATCC	Cat#300192/p777_HEK293; RRID:CVCL_0045
<b>Experimental Models: Organisms/Strains</b>		
DBA2	Charles River	N/A
C57BL/6	Charles River	N/A
B6D2F1 (DBA2xC57BL/6)	Instituto de Neurociencias de Alicante, Spain	N/A
Zic2 <sup>kd/kd</sup> (B6.129S4-Zic2 <sup>tm1Jarujaru</sup> /Jarujaru <i>Mus musculus</i> )	RIKEN Repository	IMSR Cat#RBRC00165; RRID:IMSR_RBRC00165
Unc5c <sup>rcm</sup> (B6C3Fe a/a-Unc5c <sup>rcm</sup> /J <i>Mus musculus</i> )	Jackson Laboratories	IMSR Cat#JAX:001607; RRID:IMSR_JAX:001607
Pigmented ferrets ( <i>Mustela putorius furo</i> )	Euroferret	N/A

(Continued on next page)

<b>Continued</b>		
REAGENT or RESOURCE	SOURCE	IDENTIFIER
Danio Renio (strain AB)	Instituto de Neurociencias de Alicante, Spain	N/A
Gallus gallus, fertilized chicken eggs	Granja Santa Isabel (Córdoba, Spain)	<a href="http://www.granjasantaisabel.com">http://www.granjasantaisabel.com</a> ; Cat#800008
Oligonucleotides		
shRNA primer1: 5'-GATCCGAACCACCGTGACTTTGAGTTCAAGAGACTCAAAGTCACGGTGGTTCTTTTTGGAA-3'	This paper	N/A
shRNA primer 2: 5'-AGCTTTTCCAAAAAGAACCACCGTGACTTTGAGTCTCTTGAAGTCAAAGTCACGGTGGTTTCG-3'	This paper	N/A
mUnc5c primer 1: 5'-CGGCCCGAAGAATGGAGGC-3'	This paper	N/A
mUnc5c primer 2: 5'-GGTCAGCACACGGGTCGGG-3'	This paper	N/A
zUnc5c primer 1: 5'-GACACGCAGGACGCACTCAAG-3'	This paper	N/A
zUnc5c primer 2: 5'-CCCACAGGTCCAGGATCACTC-5'	This paper	N/A
cUnc5c primer 1: 5'-CGGCCCGAAGAATGGAGGC-3'	This paper	N/A
cUnc5c primer 2: 5'-GGTCAGCACACGGGTCGGG-3'	This paper	N/A
Recombinant DNA		
mNetrin-1 pBluescript	Gift from Prof. Orly RinerW (Weizmann Institute of Science, Israel)	N/A
pCAG-mUnc5c-lresEGFP	This paper	NC_0000069.6
TOPO plasmid	Thermo Fisher Scientific	Cat#451641
pCAG-GFP	This lab (previous study [59])	N/A
pSilencer2.1	Thermo Fisher Scientific	Cat#AM5760M
Software and Algorithms		
IMARIS 9.2.1	Bitplane, Zurich, Switzerland	<a href="http://www.bitplane.com">http://www.bitplane.com</a>
Fiji	ImageJ	<a href="https://fiji.sc">https://fiji.sc</a>
MATLAB	MathWorks	<a href="https://www.mathworks.com">https://www.mathworks.com</a> ; <a href="https://github.com/SalvadorSala/SOM">https://github.com/SalvadorSala/SOM</a>
Other		
DAPI staining	Sigma-Aldrich	Cat#10236276001
Dil crystals	Thermo Fisher Scientific	Cat#D3911

## CONTACT FOR REAGENT AND RESOURCE SHARING

Further information and requests for resources and reagents should be directed to and will be fulfilled by the Lead Contact, Eloísa Herrera ([e.herrera@umh.es](mailto:e.herrera@umh.es)).

## EXPERIMENTAL MODEL AND SUBJECT DETAILS

B6D2F1 (DBA2—C57BL/6) mice used for electroporation, *in situ* hybridization, immunofluorescence or Dil tracing experiments were housed in a timed-pregnancy breeding colony at the Instituto de Neurociencias de Alicante, Spain. Zic2 knockdown mice (Zic2<sup>kd/kd</sup> mice) were originally obtained from the RIKEN Repository. Unc5c knockout mice (Unc5c<sup>rcm</sup>) were obtained from Jackson Laboratories (Stock Number: 001607). Females were checked for vaginal plugs at approximately noon each day. E0.5 corresponds to the day when the vaginal plug was detected, with the assumption that conception took place at approximately midnight. Conditions and procedures were approved by the IN Animal Care and Use Committee and met European (2013/63/UE) and Spanish regulations (RD 53/2013).

Fertilized chicken embryos were obtained from Granja Santa Isabel, Córdoba, Spain. Eggs were incubated on their sides in a humidified incubator at 37°C until the desired embryological stage. All embryos were staged according to Hamburger and Hamilton [60].

Zebrafish were maintained at 28°C under standard conditions, and the embryos were staged as described previously [61].

Pigmented sable ferrets (*Mustela putorius furo*) were obtained from Euroferret (Copenhagen, Denmark) and kept at the Animal Facilities of the Universidad Miguel Hernández on a 16:08 h light:dark cycle. Ferrets were treated according to Spanish

and European Union regulations, and experimental protocols were approved by the Institutional Animal Care and Use Committee of the University.

## METHOD DETAILS

### Plasmids

Unc5c coding sequence was cloned in the mammalian expression plasmid pCAG. Unc5c shRNA target sequence were designed using the GenScript siRNA Target Finder tool located at <https://www.genscript.com/ssl-bin/app/rnai> and cloned into the pSilencer2.1 plasmid using the pSilencer Kit (Thermo Fisher Scientific) in accordance with the manufacturer's recommendations. Mouse Unc5c RNAi target sequence was cloned using the following primers:

5'-GATCCGAACCACCGTGACTTTGAGTTCAAGAGACTCAAAGTCACGGTGGTTCTTTTTGGAA-3' and 5'-AGCTTTTCCAAAAAGAACCACCGTGACTTTGAGTCTCTTGAAGTCAAAGTCACGGTGGTTCG-3'.

### In utero electroporation and Dil tracing

Plasmidic DNA solution was injected into embryonic retinas as described previously [59, 62]. Forward Dil labeling in P0 ferret and E16.5 mice was performed as described previously [63]. After 6 days at 37°C for mice and 45 days at 37°C for ferrets, brains were removed and the optic chiasm exposed in whole mount under a fluorescence dissecting microscope. Dil crystals were dissolved in dimethyl sulfoxide and injected into the retina of 36–48 hours postfertilization (hpf) zebrafish embryos using a micropipette.

### CTB injections and adenovirus infection

Cholera toxin B subunit (CTB)-Alexa 594, 647 or 488 (Thermo Fisher Scientific) retrograde injections in P1, P3 and P28 in mouse and P1 ferret were performed as described [64]. For viral infection into the embryonic mouse retinas adenoviruses encoding for tdTomato (pAAV-CAG-tdTomato, Addgen#59462-AAV5) were injected into the retinas of E13.5 embryos following a surgical protocol similar to that used for in utero electroporation.

### Western Blot

Immunoblotting was performed to assess the presence of Unc5c and DCC across retinal development. HEK cells transfected with a Unc5c encoding plasmid and retinas from E13.5, E14.5, E15.5, E16.5, E18.5 and P2 were dissected and homogenized in lysis buffer (IGEPAL, cOMplete Mini EDTA-free protease inhibitor cocktail tablets (Sigma-Aldrich) in PBS 1x pH 7.4) and passed through a 1 mL insulin syringe with a 20G needle. Insoluble materials were incubated (30 min on ice) and pelleted by centrifugation at 16000 g for 15 min at 4°C. Protein concentration was assayed with protein assay dye reagent concentrate (BioRad) and samples were boiled in Laemmli's buffer (Sigma-Aldrich) and loaded in a gel according to standard protocols. Antibodies anti- $\beta$ -actin (Sigma-Aldrich), anti-DCC (Santa Cruz), anti-Unc5c (Abcam) were used.

### In situ hybridization and immunohistochemistry

E12.5 mouse embryos were extracted from the pregnant mother and fixed by immersion with 4% paraformaldehyde (PFA) in phosphate buffer saline (PBS, pH 7.4). Later stages embryos were intracardially perfused. Mouse and ferret heads, chicken embryos and zebrafish were post-fixed in the same fixative for 4 hours, and washed in PBS three times. The tissue was cryoprotected in 30% (w/v) sucrose in PBS and frozen in dry ice. Coronal sections (20  $\mu$ m) were obtained with a cryostat (SLEE medical GmbH, Mainz) and stored at -20°C until used. *In situ* hybridization was performed according to reported methods [65]. A riboprobe to detect mouse and ferret Unc5c mRNA was synthesized using the following primers: 5'-CGGCCCGAAGAATGGAGGC-3' and 5'-GGTCAGCACAAACGGGTCGGG-3' from E14.5 mouse embryos cDNA. To detect zebrafish Unc5c mRNA we used a riboprobe cloned in a TOPO plasmid (Thermo Fisher Scientific) from zebrafish cDNA at 36–48 hpf using the following primers: 5'-GACACGCAGGACGCACTCAAG-3' and 5'-CCCACAGGTCCAGGATCACTC-5. To detect chicken Unc5c mRNA a riboprobe, cloned in a TOPO plasmid, was synthesized using the following primers: 5'-CGGCCCGAAGAATGGAGGC-3' and 5'-GGTCAGCACAAACGGGTCGGG-3' from E7 chicken embryos.

Netrin1 was detected using a specific antisense riboprobe (gift of Prof. Orly Reiner (Weizmann Institute of Science, Rehovot, Israel)). For immunohistochemistry, antigen retrieval was performed before blocking and incubation with specific primary antibodies. The following primary antibodies were used: chicken anti-GFP (Aves Labs); rabbit anti-Zic2 (Herrera's lab [55–58]); mouse anti-Tuj1 (Covance), rabbit anti-Tuj1 (Abcam), mouse anti-Brn3a (Chemicon), rabbit anti-calbindin (Swant), goat anti-ChAT (Millipore). For immunofluorescence detection, Alexa 488, Alexa 546, and Alexa 647 (Invitrogen, Molecular Probes) secondary antibodies were used. A DAPI staining solution was used to visualize nuclei (2  $\mu$ g/mL).

### Microscopy setup

Images were captured with an Olympus FV1000 confocal IX81 microscope/FV10-ASW software. Deconvoluted z stack images data acquired from tissue section by confocal microscopy were rendered in three dimensions using IMARIS 9.2.1 (Bitplane, Zurich, Switzerland). Chiasm images were acquired using a Leica MZ16F stereoscope.



### Mathematical Model

We generated a simplified version of the self-organizing map (SOM) model originally described by [37–39]. The topography of the RGCs is represented by a regular square mesh of size 11 by 11 with the cells in the nodes. Those cells project to a postsynaptic layer of the same size, initially with synapses connecting all pre- and postsynaptic neurons in a non-specific manner. Thus, a representation of the location of the center of mass (CM) of the normalized weights,  $w$ , of the synaptic connections results in a mesh contained in a unit square (Figure S5). The model incorporates the role of the gradients of molecular guidance cues in establishing topography as a Gaussian function which sets the strength of the initial weights of the synaptic connections, based on the proximity between the presynaptic and postsynaptic neurons as,

$$MG = e^{-\frac{\| (r_{pre} + r_{noise1}) - (r_{post} + r_{noise2}) \|^2}{2 \cdot \sigma_{molecular}^2}}$$

where MG is the weight of the molecular gradient for each presynaptic neuron respect to all of the postsynaptic neurons,  $\sigma_{molecular}$  determines the specificity or strength of the molecular gradient and  $r_{noise}$  introduces a level of normally distributed noise between connections, with mean 0 and standard deviation  $\sigma_{noise}$  (Figure S5).

By stimulating the retina with different stimuli (see below), the synaptic weights change according to a Hebbian rule as follows:

$$\delta w_i = \lambda \cdot e^{-\frac{t}{\tau}} \cdot e^{-\frac{(X-x_w)^2 + (Y-y_w)^2}{2\sigma^2}} \cdot (r_s - w_i)$$

where  $\delta w_i$  is the change in the  $i$  synaptic weight  $w_i$ ,  $\lambda$  is the weight decay term,  $t$  is the time expressed in number of iterations,  $\tau$  is the time constant for the  $\lambda$  decay,  $X$  and  $Y$  are the arrays holding the coordinates of retinal ganglion cells,  $x_w$  and  $y_w$  are the coordinates of the cell closest to the stimulus location which will receive the strongest effect,  $\sigma$  gives the extent to which the activation propagates to neighboring cells, and finally,  $r_s$  is the vector containing the positions of the stimulus.

The different types of retinal activity used are shown in Figure S6. First, random patterns activate each retina with a sequence of independent uniform random stimuli. This stimulus class models the emergence of retinotopic topography in the absence of R-R projections. Second, locally coupled stimuli activate synchronously a small subset of RGCs retinotopically matched in both retinas for the first few iterations (100) of the model. Afterward, the activation of both retinas followed a sequence of independent uniform random stimuli as in the previous scenario. Last, binocularly matched retinal waves were triggered near the center of a retinal mesh and travel toward the periphery at the same speed in both retinas. The radius of the wave of stimulation increased at a rate of  $2 \cdot 10^{-4}$  (per iteration), and stimuli were applied randomly around that radius following a Gaussian distribution of mean 0 and sigma 0.04. In each case, the final synaptic strength onto each postsynaptic neuron  $N_i$  is the normalized average of all of its weighted connections. By modeling the development of the right and left postsynaptic targets simultaneously, we were able to study how the presence or absence of R-R connections, and the different patterns of coordinated activity that they afford, could affect the establishment of bilaterally congruent retinotopic maps in visual structures receiving direct retinal inputs (Figure S6). The model returns correct results, i.e., perfectly matched left and right retinotopic layouts, only when the unfolding and orientation of both postsynaptic sheets is the same as the orientation in the presynaptic RGC layer. On the other hand, incorrect results could come in the form of different orientations between pre and postsynaptic sheets or incorrect unfolding, which produce disruptions on the topographic map. Model parameters and code are provided in Table S1 of the accompanying Supplemental Information and Software and Algorithms in the STAR Methods section.

### QUANTIFICATION AND STATISTICAL ANALYSIS

To quantify retinal projections at the optic chiasm level, squared regions of interest (ROI) were superimposed on the width of the optic nerve close to the electroporated retina, the opposite optic nerve, the contralateral optic tract and the ipsilateral optic tract in regions proximal to the chiasm. Fluorescence intensity within each ROI was measured using ImageJ Software and normalized with respect to the background. The percentage of fluorescence intensity in each ROI relative to the optic nerve ROI on the electroporated side was then represented in a graph. Statistical analyses were performed when appropriate, error bars indicate  $\pm$  SEM (\* $p < 0.05$ , \*\* $p < 0.01$ , \*\*\* $p < 0.001$ , Student's unpaired t test)

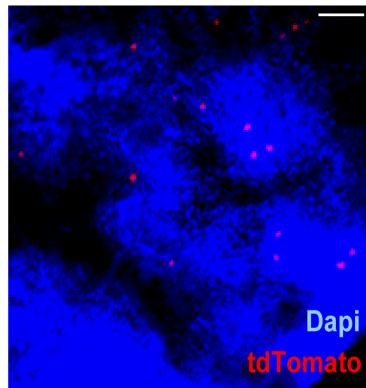
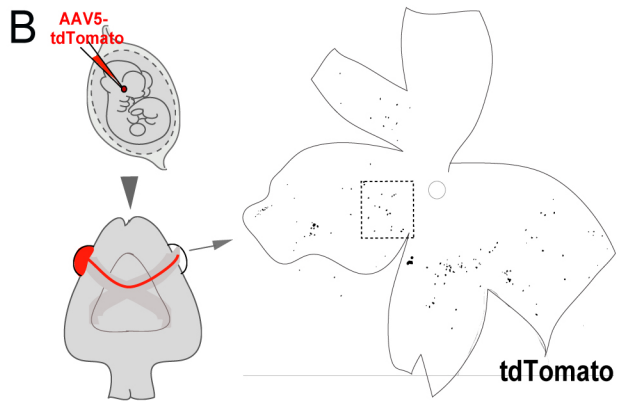
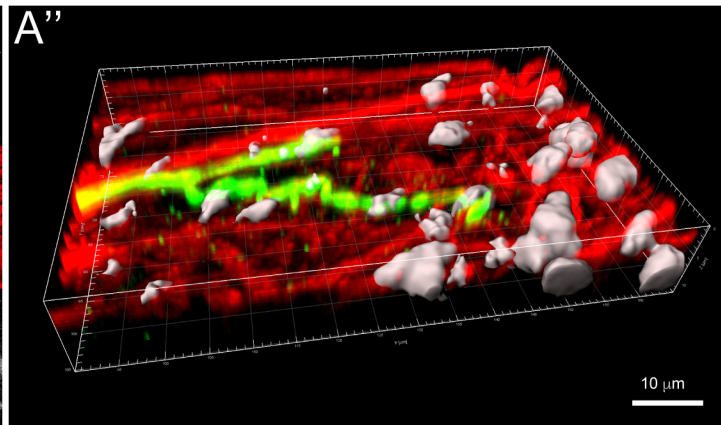
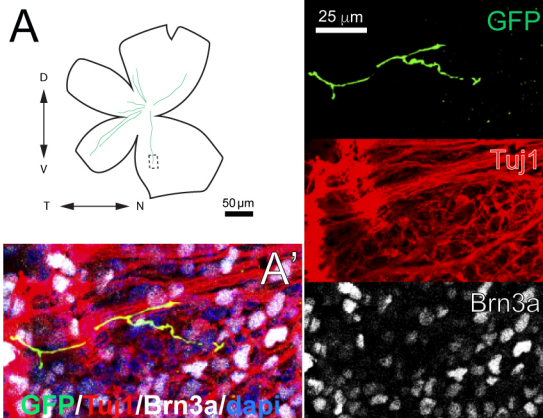
**Current Biology, Volume 29**

**Supplemental Information**

**A Retino-retinal Projection Guided by Unc5c**

**Emerged in Species with Retinal Waves**

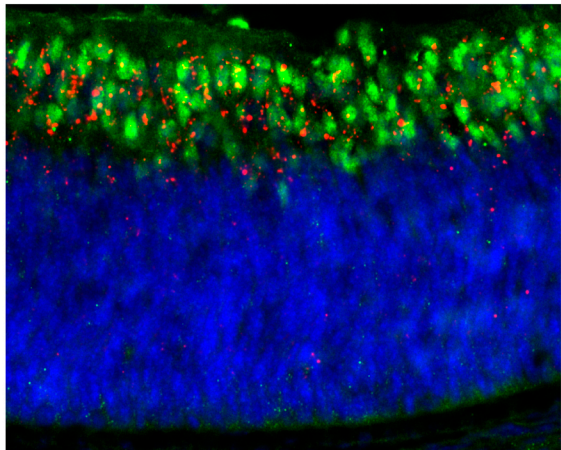
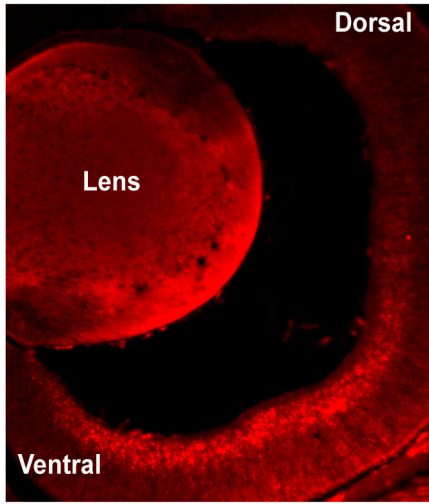
**Verónica Murcia-Belmonte, Yaiza Coca, Celia Vegar, Santiago Negueruela, Camino de Juan Romero, Arturo José Valiño, Salvador Sala, Ronan DaSilva, Artur Kania, Víctor Borrell, Luis M. Martínez, Lynda Erskine, and Eloísa Herrera**



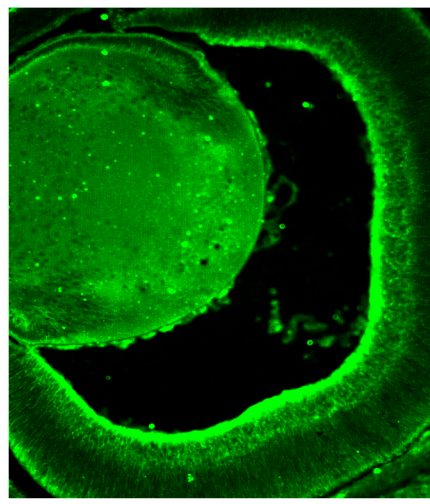
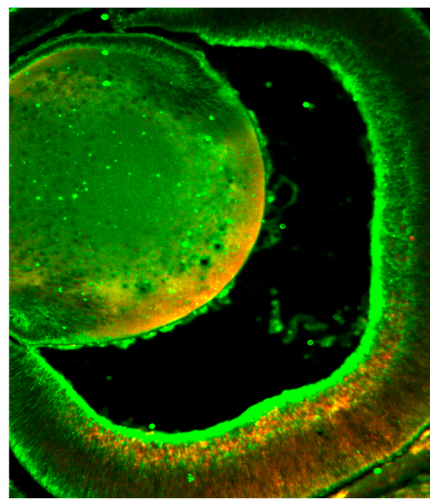
**Figure S1. Characterization of the R-R projection. Related to Figure 1.**

(A) Drawing of a P2 retina containing R-R axons labeled by electroporation at E.13.5. (A') High magnification of the boxed region in (A) showing an eGFP-R-R axon terminal in a retina incubated with Tuj1 (red) and Brn3b (white) antibodies. The three channels are shown separately at the right. (A'') 3D reconstruction of a z-stack captured from the boxed area in "A".

(B) Retrograde labeling by AAV5-infection. The drawing at the left summarizes the experimental procedure for retrograde viral infection. AAV5-tdTomato viruses (red) were injected into one retina of E13.5 embryos and 10 days later the contralateral retina was analyzed. The color-inverted whole-mounted retina at the right shows the distribution of RGCs retrogradely labeled from a P5 pup injected with the AAV5-tdTomato virus at E13.5. The td-Tomato cells are located predominately at the ventral part of the central retina. Image at the right, higher magnification of the boxed region.

**A***Unc5c mRNA*/Brn3a/dapi**B***Unc5c mRNA*

DCC

*Unc5c mRNA*/DCC

**Figure S2. *Unc5c* and *DCC* expression in the developing retina. Related to Figure 3.**

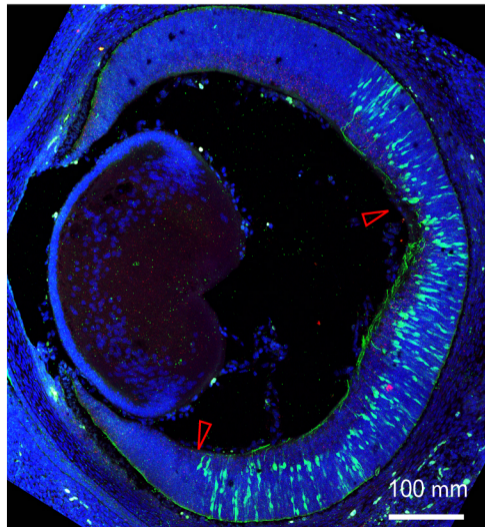
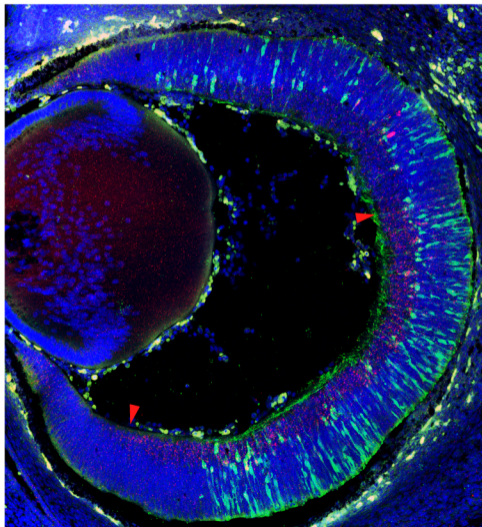
(A) Immunohistochemistry for Brn3a (green) combined with ISH for *Unc5c* (red) in a coronal section through an E16.5 mouse retina counter stained with dapi (blue). *Unc5c* is expressed in the RGC layer.

(B) Immunostaining for Dcc (green) combined with ISH for *Unc5c* (red) in a coronal section through an E15.5 mouse retina.

control shRNA+eGFP

Unc5c shRNA+eGFP

mRNA *Unc5c*/dapi/eGFP

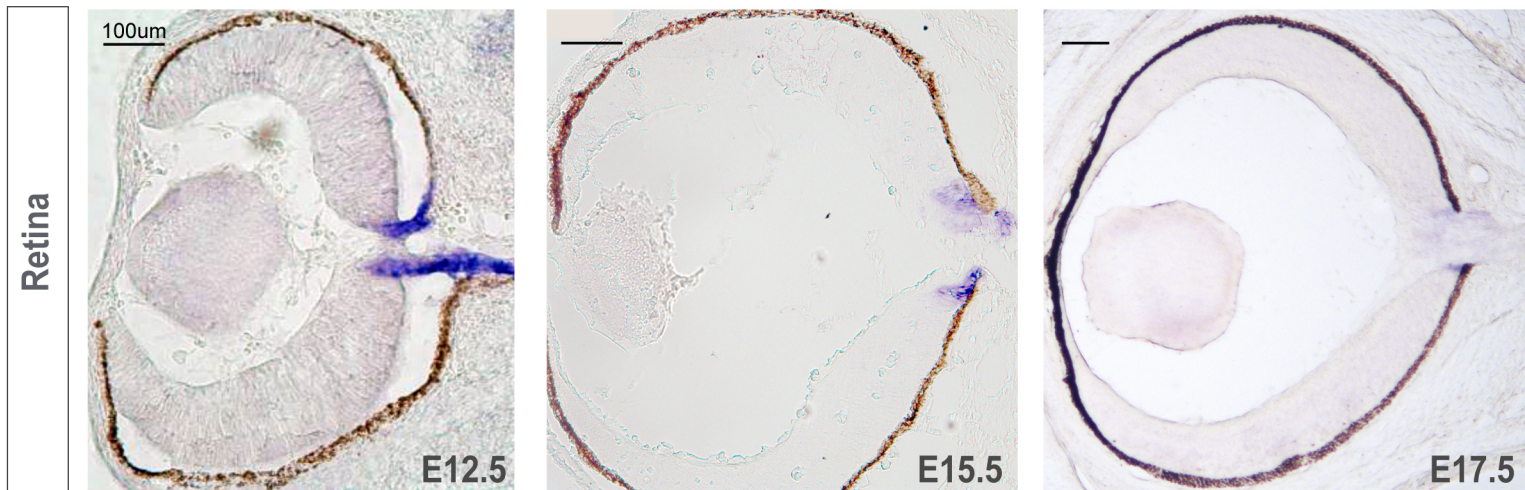


**Figure S3. Downregulation of retinal *Unc5c* by shRNA electroporation. Related to Figure 4.**

ISH for *Unc5c* (red) in coronal retinal sections from E16.5 embryos electroporated at E13.5 with control shRNA+eGFP or *Unc5c* shRNA+eGFP (green) and counter stained for DAPI (blue). After electroporation of *Unc5c* shRNA+eGFP, *Unc5c* expression (open arrowheads) is downregulated compared to the control retinas (red arrowheads).



A

*Netrin mRNA*

B

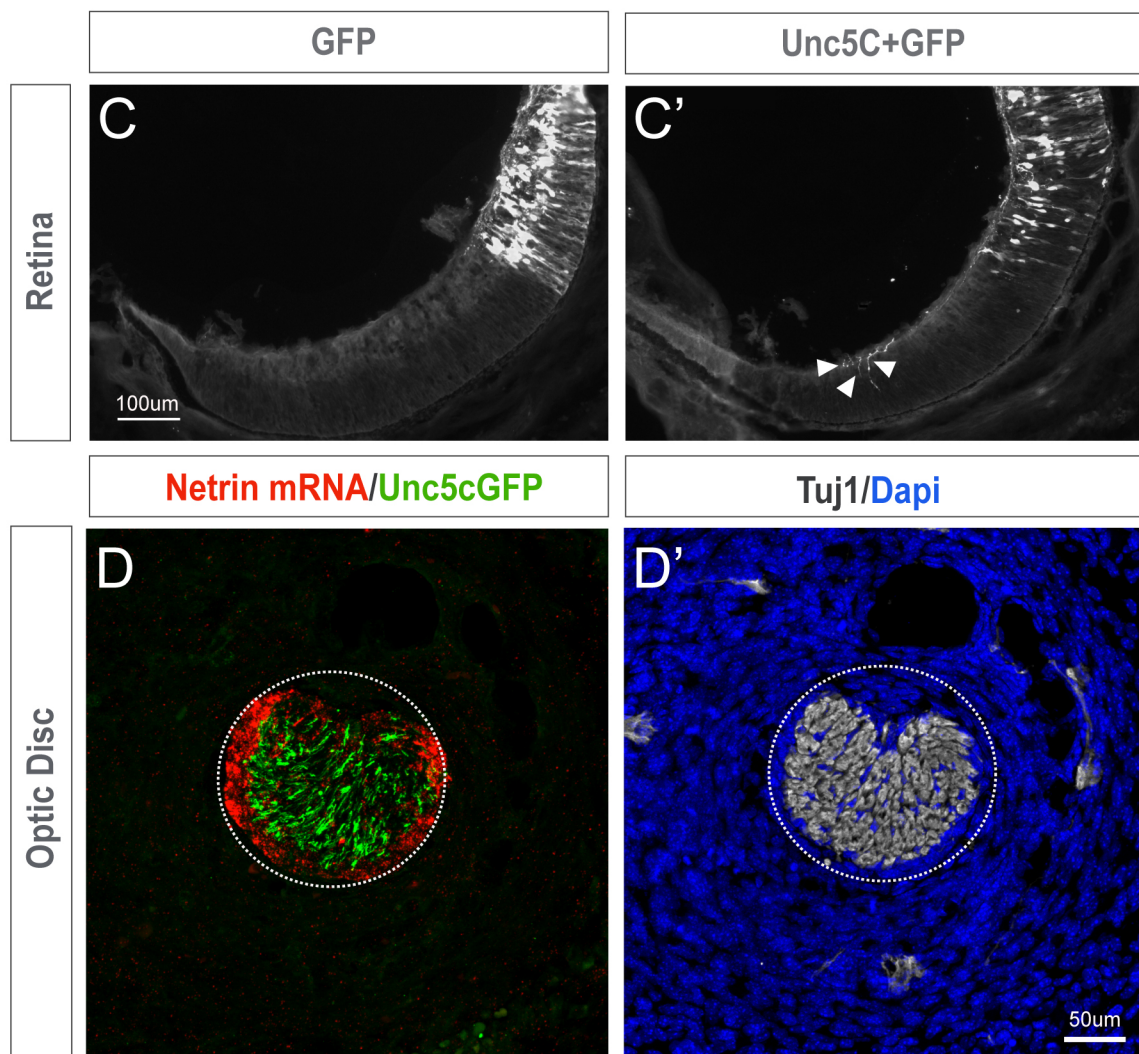
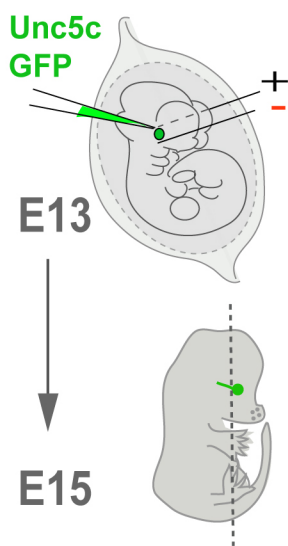


**Figure S4. *Netrin* expression and intraretinal guidance in *Unc5c* electroporated retinas. Related to Figure 6.**

(A) ISH for *Netrin1* in coronal sections through E12.5 – E17.5 wild-type retina. At E12.5 *Netrin1* is highly expressed in the optic stalk. At later stages (E15.5-E17.5) *Netrin1* expression at the optic stalk decreases.

(B) eGFP or *Unc5c*/GFP encoding plasmids were electroporated into one eye of E13.5 embryos and axon trajectory analysed at E15.5.

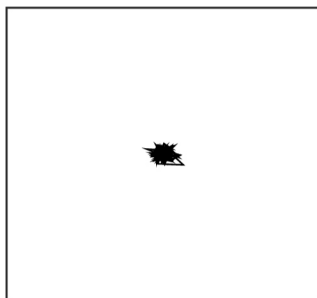
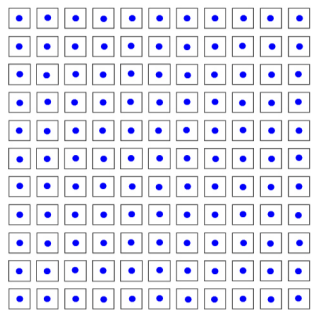
(C-C') In control embryos, eGFP electroporated RGCs send their axons through the optic disc

(C). In embryos electroporated with *Unc5c*/GFP some labelled RGCs misproject inside the retina, rather than exiting the eye (arrowheads, C').

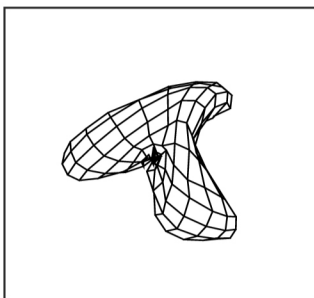
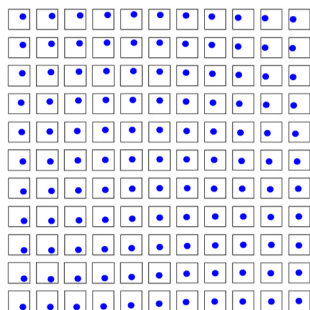
(D-D') ISH for *Netrin1* in a transversal section throughout the optic disc of an E15.5 embryo electroporated at E13.5 with *Unc5c*/GFP encoding plasmids. (D) Despite *Netrin1* expression in the optic disc, many axons expressing *Unc5c*/GFP are able to exit the retina growing through the *Netrin1* ring surrounding the optic disc. (D') Tuj-1 and dapi stainings in the same section as (D) to visualize RGC axons exiting the retina and the anatomy of the optic disc.

A

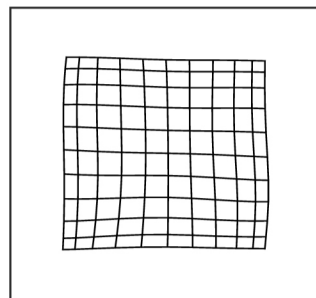
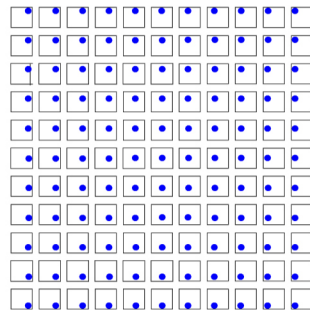
0



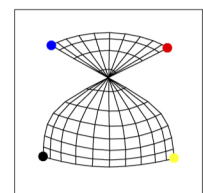
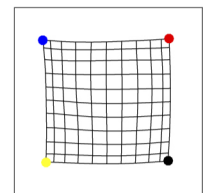
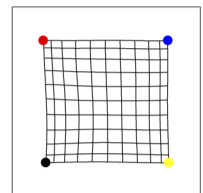
100



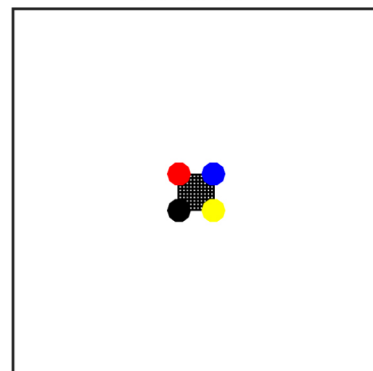
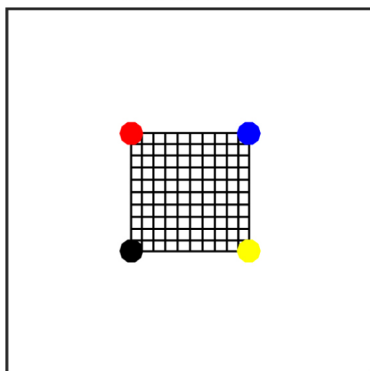
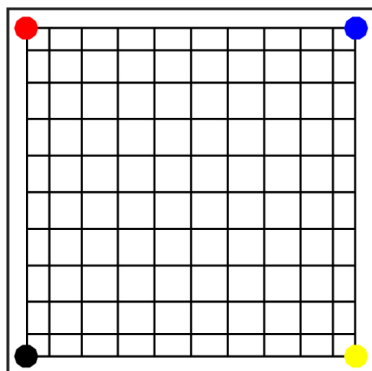
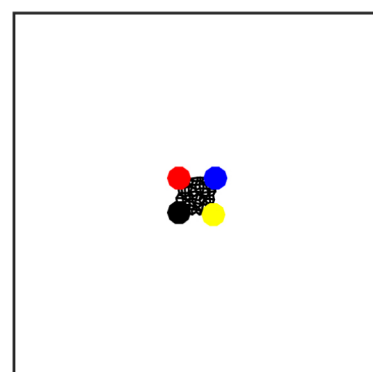
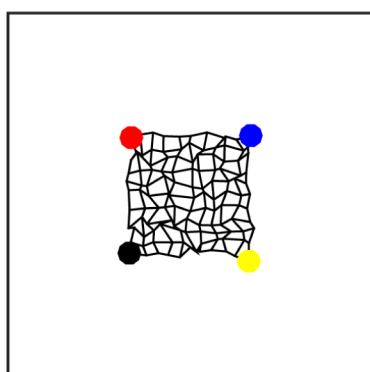
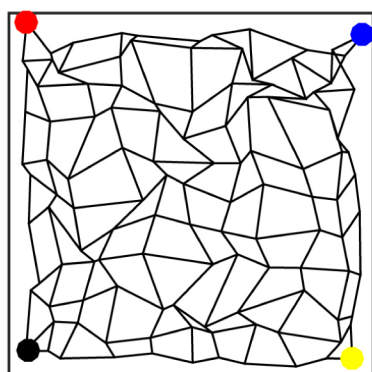
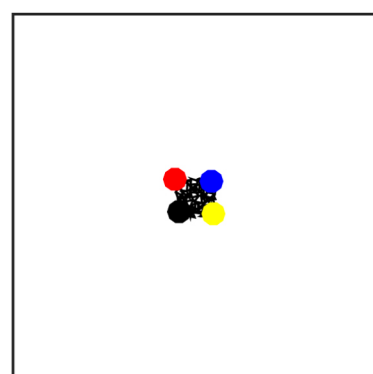
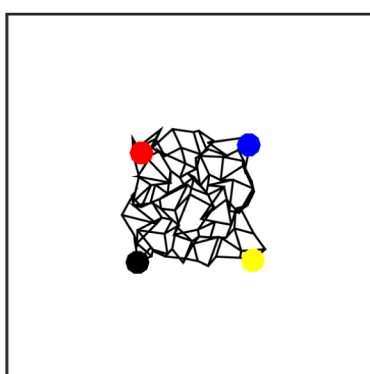
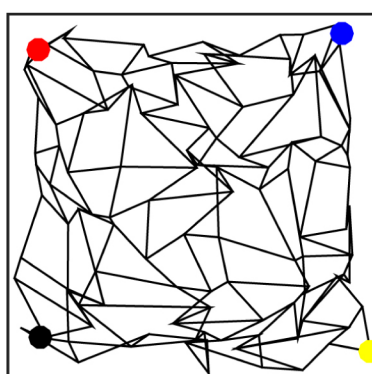
12000



B



C

 $\sigma_{\text{molecular}}=0.1$  $\sigma_{\text{molecular}}=0.5$  $\sigma_{\text{molecular}}=1$  $\sigma_{\text{noise}}=0$  $\sigma_{\text{noise}}=0.03$  $\sigma_{\text{noise}}=0.06$ 

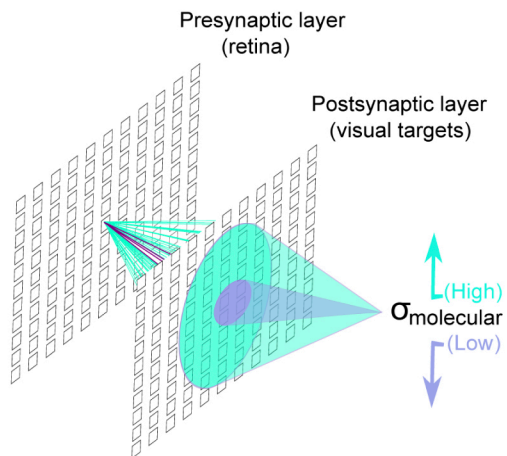
**Figure S5. The SOM model generates topographic maps. Related to Figure 7.**

(A) Top row: position of center of receptive field for each postsynaptic cell. Bottom row: position of center of mass of synaptic connections. Left panel: at time 0, all synaptic weights are distributed equally, so that postsynaptic neurons response is not specific. Center panel: at time 100 postsynaptic responses and weights become more specific. Right panel: at time 12000 an ordered topographic map has emerged.

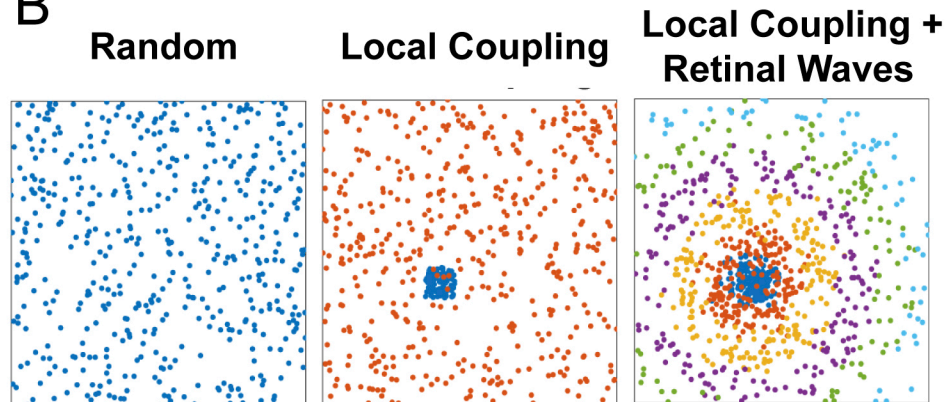
(B) The model returns different final results after 12000 iterations. Top: the postsynaptic sheet develops the same orientation as the presynaptic sheet, as indicated by the location of the colored corners. Center: the map unfolds but with incorrect orientation, different from the retina. Bottom: The postsynaptic weights did not unfold properly (the retinotopic map is disrupted). Thus, the map develops overtime from a condition in which all cells are connected with almost equal weights, so that the position of all receptive fields is very close to the center, to a situation in which, after 12000 cycles of stimulation, the synaptic connections have been greatly refined and the receptive fields of each post-synaptic cells relocated to form an orderly topographic map.

(C) Effect of molecular gradient and positional noise in the development of retinotopic maps. Initial maps for all combinations of  $\sigma_{\text{molecular}} \in [0.1, 0.5, 1]$  and  $\sigma_{\text{noise}} \in [0, 0.03, 0.06]$ . The effect of the model parameters  $\sigma_{\text{molecular}}$  and  $\sigma_{\text{noise}}$  is illustrated. A low value of dispersion in the molecular gradient and noise level gives an initial mesh very close to a perfectly deployed topographic map (upper left panel). Increasing the value of  $\sigma_{\text{noise}}$  (top to bottom in the figure) produces more disorganized initial maps. Increasing the value of  $\sigma_{\text{molecular}}$  (left to right in the figure) produces less predetermined initial maps, with receptive fields for all cells very close to a uniform response, and the positions of the center of mass of the weights very close to the center.

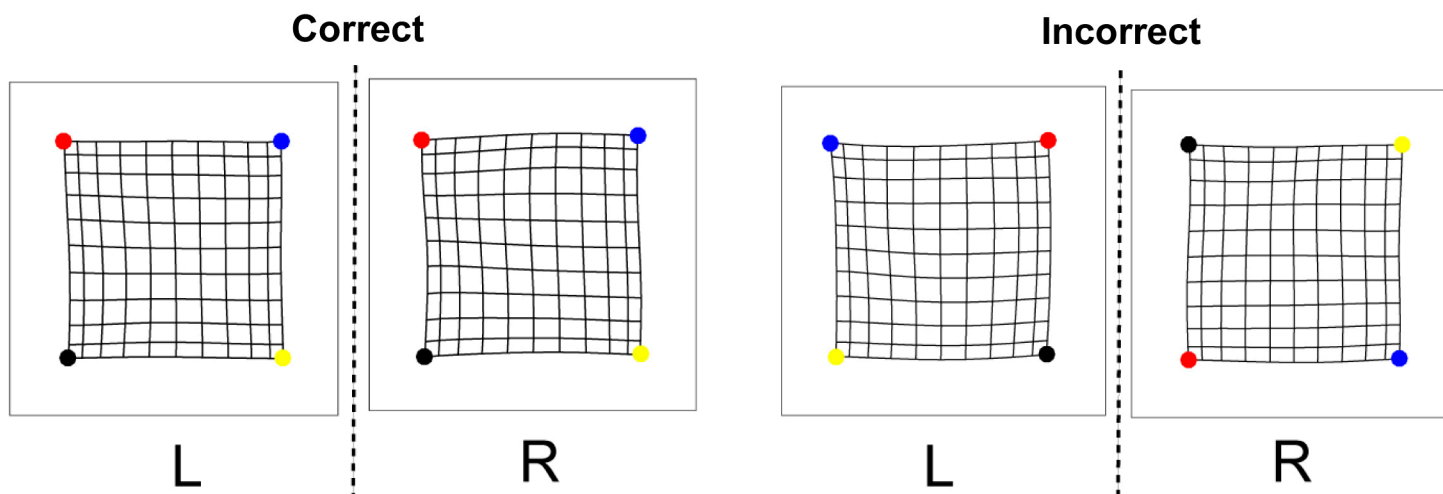
A



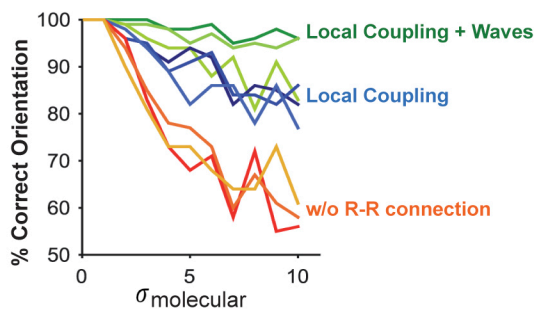
B



C



D



E

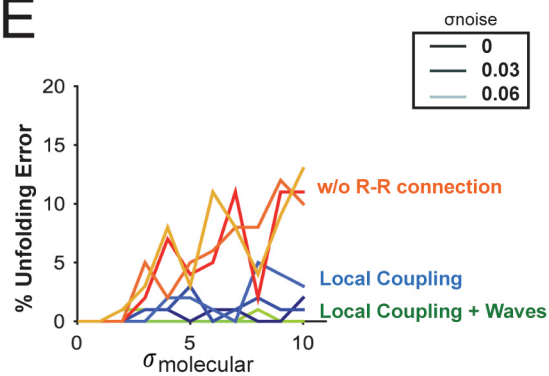


**Figure S6. Effect of molecular- and activity-dependent mechanisms on the development of bilaterally congruent topographic maps. Related to Figure 7.**

(A) A gradient of different guidance molecules instructs initial targeting in the postsynaptic layer. To simulate the initial spread of the axons, the effect of the molecular gradient ( $\sigma_{\text{molecular}}$ ) was modelled as a Gaussian function which increased the strength of the initial weights in the model based on the proximity of the presynaptic and postsynaptic neurons. Accordingly, high  $\sigma_{\text{molecular}}$  values increased the initial spread of the axons, while low  $\sigma_{\text{molecular}}$  values generated a lower initial coverage.

(B) Left panel: To model the absence of R-R connections, a set of completely random stimuli was applied. Center and right panels: The presence of R-R connections was modeled in two different ways: Local coupling - an initial region of stimulation (shown in blue) is followed by random activity. Local coupling + retinal waves - local coupling followed by a retinal wave traveling at a constant velocity.

(C) Retinotopic maps in mice have bilateral congruency, thus both topographic maps are arranged in the same orientation. By modelling the development of the right and left postsynaptic targets simultaneously, we were able to study the role of molecular guidance cues and synchronous activity in the development of bilateral congruency.

Examples of two simulations. Left: Correct bilateral congruency, i.e., left (L) and right (R) postsynaptic layers develop the same orientation as the presynaptic sheet as indicated by the order of the colored dots in the corners. Right: Incorrect bilateral congruency, in which, neither of the postsynaptic sheets coincides with the orientation of the retina nor coincide with each other as indicated by the order of colored dots.

(D) Percentage of maps with the correct orientation in both eyes (as a function of molecular gradients,  $\sigma_{\text{molecular}}$ ), for the three types of stimuli (random stimulus that corresponds to no R-R connection (red), local coupling stimulus (blue) and local coupling plus retinal wave stimulus (green)). Noise levels are represented with different shades of the same color and correspond to  $\sigma_{\text{noise}}$ : 0, 0.03 and 0.06.

(E) Percentage of maps with topological defects or unfolding errors as a function of the molecular gradient for the three types of stimuli and the three different noise levels.

*mRNA Unc5c*

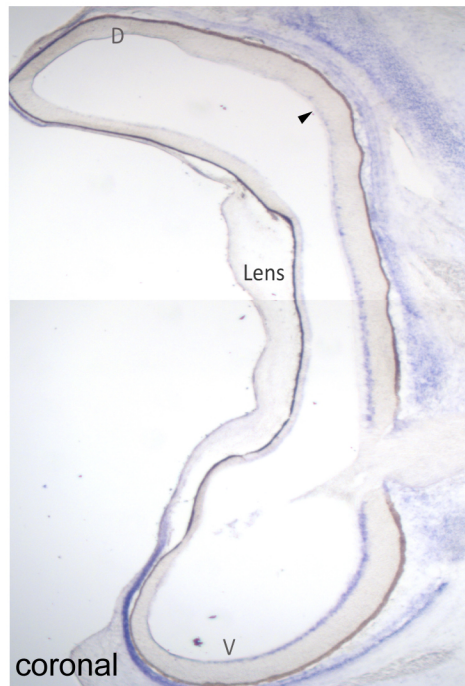


**Figure S7. *Unc5c* expression in the developing chicken retina. Related to Figure 7.**

Colorimetric ISH for *Unc5c* in horizontal and coronal sections of E7 chicken retinas. *Unc5c* is expressed in the RGC layer in a ventrocentral pattern similar to *Unc5c* expression in mouse and ferret. D, dorsal, N, nasal, T, temporal, V, ventral.



Parameter	Description	Value
$\lambda$	Weight decay term	0.1
$\tau$	Time constant of $\lambda$ decay	5555
$\eta t$	Number of iterations	12000
$\sigma_\alpha$	Lateral interaction influence	2
$\eta\eta$	Number of cells	11 x 11
$\sigma_{noise}$	Standard deviation (SD) of position noise	[0,0.21]
$\sigma_{molecular}$	SD of the molecular gradient	[0.1,10]

**Table S1. Numerical values of model parameters. Related to Mathematical Model in STAR Methods and Figure S6.**